Construction and Building Materials 387 (2023) 131617

Contents lists available at ScienceDirect

Construction and Building Materials

journal homepage: www.elsevier.com/locate/conbuildmat

A self-sensing and self-heating planar braided composite for smart civil infrastructures reinforcement

Mohammadmahdi Abedi [a,b,c], Usha Kiran Sanivada [c,d,e], Seyed Ali Mirian [f], Omid Hassanshahi [a,b,c], Khalifa Al-Jabri [g], António Gomes Correia [a,b], Paulo B. Lourenço [a,b], Raul Fangueiro [c,d,e,*]

[a] Department of Civil Engineering, University of Minho, Campus de Azurém, 4800-058 Guimarães, Portugal
[b] Institute for Sustainability and Innovation in Structural Engineering, University of Minho, 4800-058 Guimarães, Portugal
[c] Fibrenamics, Institute of Innovation on Fibre-Based Materials and Composites, University of Minho, 4800-058 Guimaraes, Portugal
[d] Department of Mechanical Engineering, University of Minho, Campus de Azurém, 4800-058 Guimarães, Portugal
[e] Centre for Textile Science and Technology, School of Engineering, University of Minho, 4800-058 Guimarães, Portugal
[f] Department of Mechanical Engineering, Isfahan University of Technology, 84156-83111 Isfahan, Iran
[g] Department of Civil & Architectural Engineering, Sultan Qaboos University, 123 Al-Khod, Oman

ARTICLE INFO

Keywords:
Self-sensing
Self-heating
Planar braided composite
Cementitious composite
Carbon nanomaterials
Polymer

ABSTRACT

Allocating different capabilities to structural elements simultaneously is still challenging. In this study, a field-applicable multifunctional planar braided composite with the abilities of reinforcing, self-sensing and self-heating was developed for the first time. In this route, three commercial fabrics were used, including cotton, cotton/polyamide, and polyester. The fabrics were first chemically treated and then coated with a carbon nanomaterial-based polymeric conductive paste using screen printing with different concentrations and layers. The samples were then covered and sealed with a thermoplastic polyurethane-based polymer to avoid environmental factors effects. Smart planar composites (SPC) were also used as reinforcement for cementitious specimens. The electrical conductivity and joule heating capability of the samples were also evaluated. The microstructure of the SPCs was investigated using various tests. The mechanical and self-sensing performances of the cementitious composite reinforced with different SPCs were assessed using different load patterns. The results showed a heating rate of 0.44 ℃/s, a joule heating power of 0.7 W/C, and a maximum temperature of 44 ℃ which proved the proper heating capability of the cementitious composites reinforced with SPCs. The great correlation between electrical resistivity changes and strain values indicated the high potential of the composite in strain sensing for different applications. The SPCs also improved the post-crack behaviour of the specimen and its flexural strength and failure strain by approximately 50% and 118%, respectively. The outcomes of this study draw a bright horizon in multifunctional braided composite development with different applications in civil infrastructures, which is a crucial step for intelligent cities' advances.

1. Introduction

The expansion of intelligent infrastructures and smart cities results from technological progress in today's world and causes a growing demand for multifunctional and smart materials in the civil construction industry [1–4]. Indeed, sensing and heating performances are among the fundamental capabilities which are the bases of many other functions and mechanisms in civil projects [5–10]. Conventionally multifunctional materials can also act as sensors which are an integrated part of monitoring systems for data harvesting (e.g. strain, deformation, stress, corrosion, damage, temperature and humidity status) at an operational level of infrastructure [11–13]. They can feed machine learning and artificial intelligence algorithms to be used for energy-associated processes, structural health monitoring, smart transportation, traffic flow, speed and weight monitoring, and driverless vehicle development [12,14–18]. Several sensing techniques including, piezoelectric ceramic, foil strain gauge, shape memory alloys, and optical fibres have been studied for civil construction monitoring [19,20]. These sensors

* Corresponding author at: School of Engineering, University of Minho, Campus de Azurém, 4800-058 Guimarães, Portugal.
E-mail address: rfangueiro@det.uminho.pt (R. Fangueiro).

https://doi.org/10.1016/j.conbuildmat.2023.131617
Received 1 February 2023; Received in revised form 27 March 2023; Accepted 29 April 2023
0950-0618/© 2023 The Authors. Published by Elsevier Ltd. This is an open access article under the CC BY-NC license (http://creativecommons.org/licenses/by-nc/4.0/).

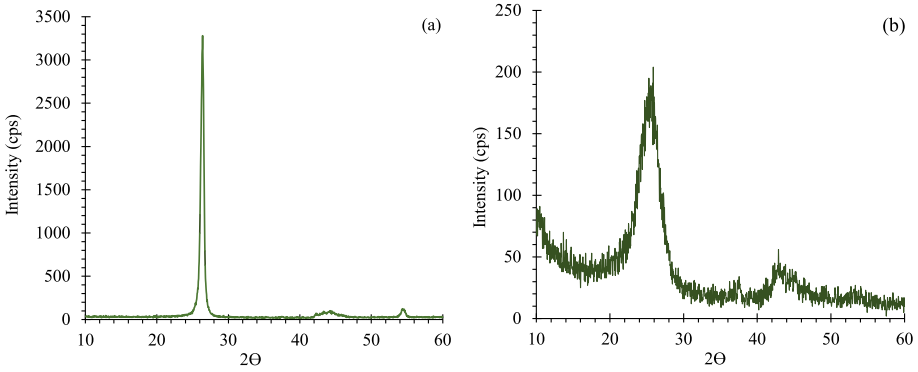


Fig. 1. The X-Ray spectra of carbon nanomaterials: a) GNPs, b) MWCNTs.

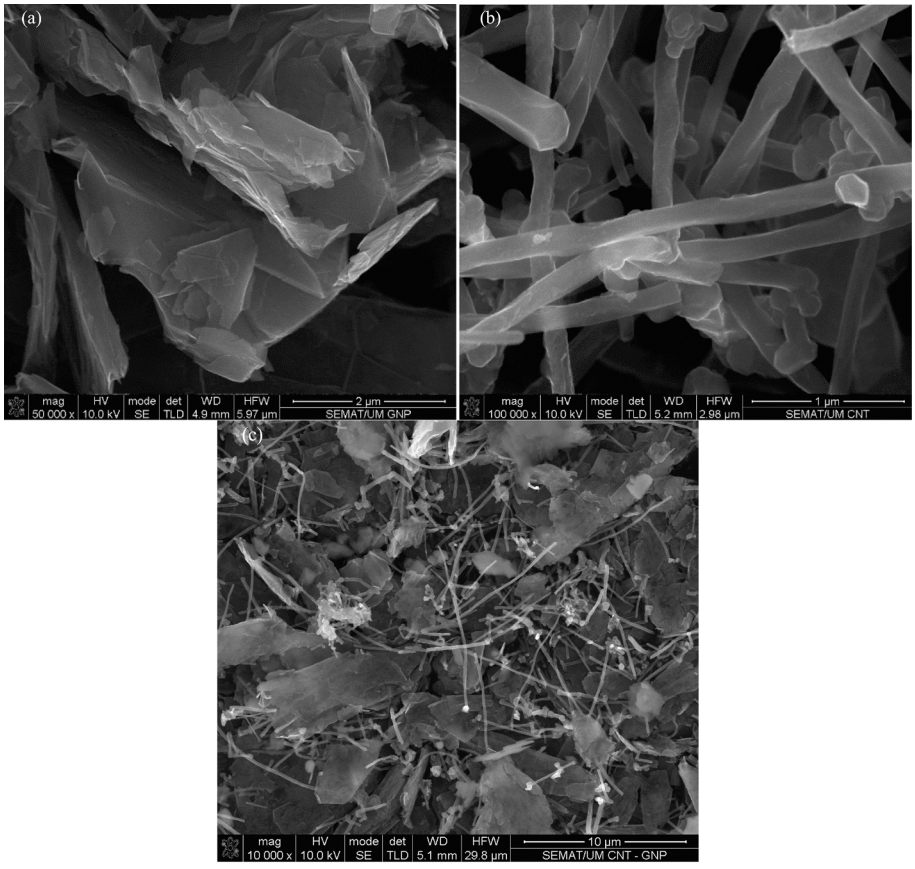


Fig. 2. The morphology of carbon nanomaterials: a) GNPs, b) MWCNTs, c) the mix of CNT/GNPs.

Table 1
The main characteristics of GNP and MWCNT used in this study.

GNP								
Surface area (m^2 g^{-1})	Density (g/cm^3)	Carbon content (%)	Tensile modulus (GPa)	PH Value (30 °C)	Tensile strength (GPa)	Layers	Dimension	Form
120–150	2.25	> 99.5	1000	7–7.65	5	< 20	Thickness 4–20 nm Diameter 5–10 μm	Grey Powder
MWCNT								
Surface area (m^2 g^{-1})	Density (g/cm^3)	Colour	Outside Diameter (nm)	Length (μm)	Ash (wt%)		Carbon content (%)	
≥380	2.17	Black	1–2	5–30	< 1.5		> 90	

Table 2
Physical properties of resins used in this study.

Physical Properties	Edolan CM	Tanapur EP 3061	Thickener A 02	Physical Properties	TPU Apilon MA52
Viscosity, 25 °C (mPas)	≤90 s (at 20°C, ISO 2431)	≤90 s (at 20°C, ISO 2431)	≤10	Tear strength (kN/m)	60
Density, 25 °C (g/ml)	1.1	1 – 1.1	1.19	Tensile modulus [1] (MPa)	2.5
Ionicity	Anionic	Slightly cationic	Non-Ionic	Tensile strength (MPa)	20
Physical form	Liquid	Liquid	Liquid	Physical form	pellets
Colour	White	Light Yellow	Light Yellow	Tensile elongation[2] (%)	800

[1] 100% Elongation, [2]At break.

Table 3
Main physical and mechanical properties of the fabrics used in this study.

Physical Properties	Cotton (C)	Cotton/Polyamide (C/PA)	Polyester (PL)
Tenacity/warp (cN/tex)	3.1	5.5	7.2
Weft density (yarns/cm^2)	26	32	38
Warp density (yarns/cm^2)	33	38	45
Extension (%)	9.7	19.1	26.4

conventionally are either applied to the external surfaces or embedded into the structure [21,22]. Dong et al. [5] provide a comparison of different monitoring techniques for concrete and cement structures. The sensors are usually incompatible with cementitious materials, reducing the structure's strength and durability [5,21,23]. Moreover, the limited monitoring scope of these techniques renders them impractical for field-scale infrastructures [24–26].

As mentioned, nowadays the heating potential of cementitious composites has received particular attention due to its function in de-

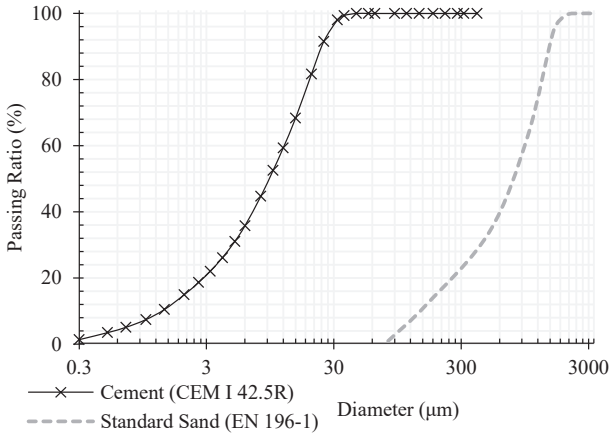


Fig. 4. Particle size distribution of the used cement and sand.

Table 4
The main physical characteristics of the sand.

Mesh Size (mm)	0.08	0.16	0.5	1	1.6	2
Cumulative retained (%)	99 ± 1	87 ± 5	67 ± 5	33 ± 5	7 ± 5	0
Specific gravity G_s	2.67		Cu[a]	7.5	Cc[b]	1.8

[a] Uniformity coefficient, [b] Curvature coefficient.

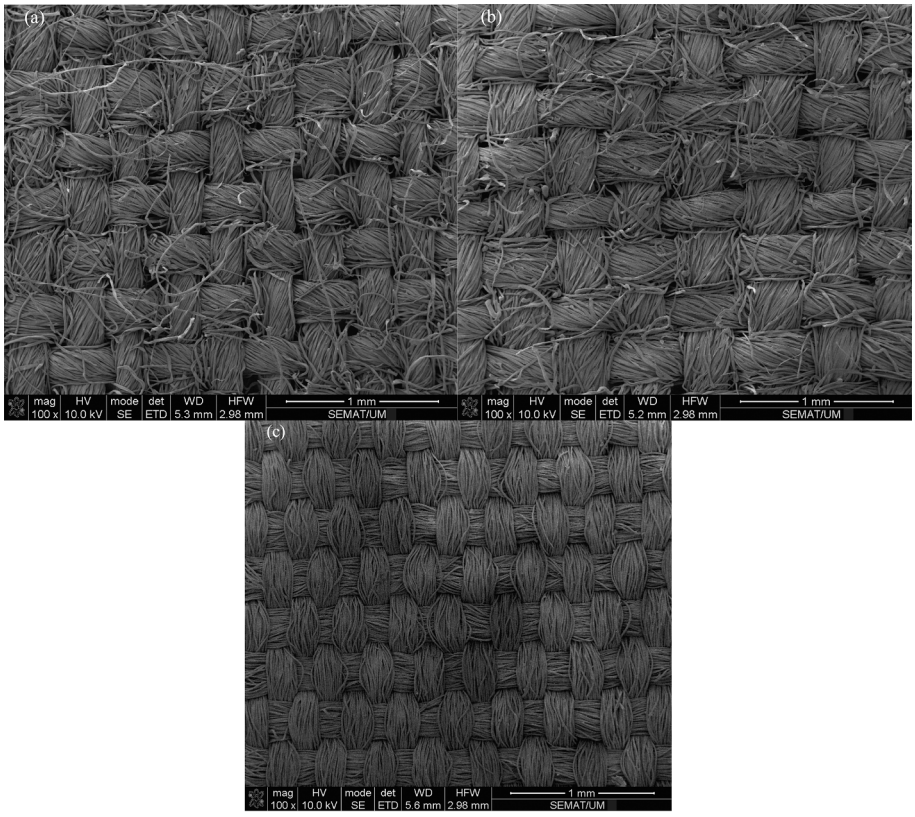


Fig. 3. Morphology of the fabrics: a) Cotton b) Cotton/Polyamide c) Polyester.

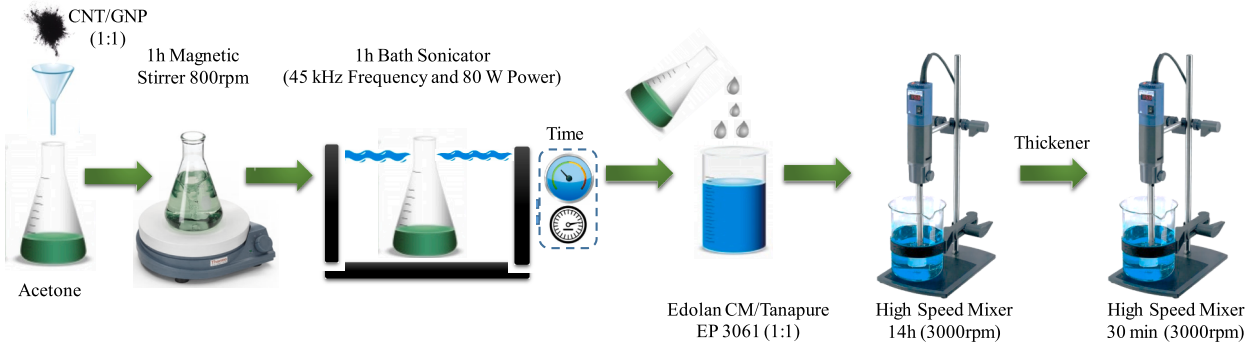


Fig. 5. A schema of the CNT/GNP dispersion process and conductive paste production steps.

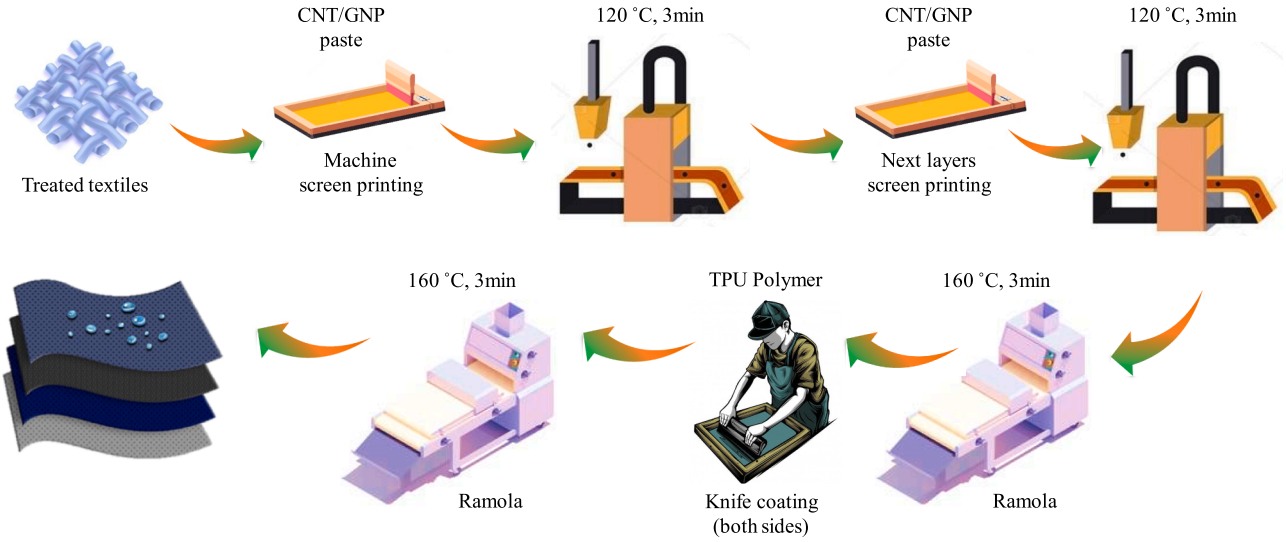


Fig. 6. The coating process of the fabrics.

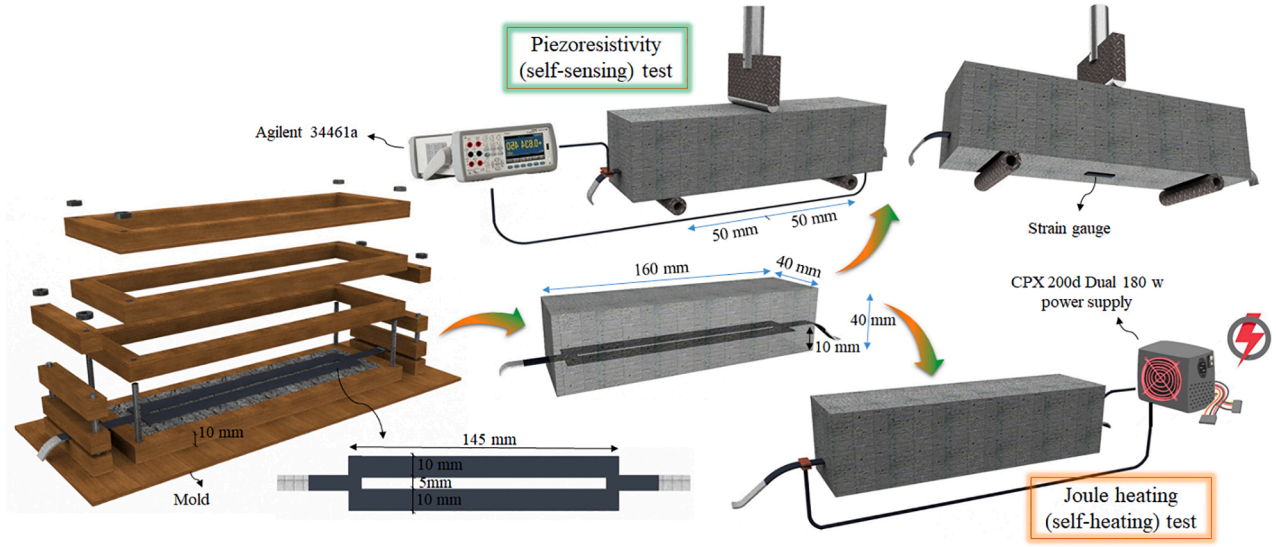


Fig. 7. Schema of cementitious composite fabrication, specimen configuration, Self-sensing and self-heating tests setup.

icing, snow-melting, common healing mechanisms, and energy-efficient applications for different infrastructural and structural elements [27–30]. Self-heating coating [31,32], built-in heating pipelines [33–35], phase-change materials [36,37], super-hydrophobic coating [38], and self-heating concrete [39–41] have been often used as active methods in previous studies to assign the heating performance to different civil structures. However, the cost of production, the low energy efficiency, and the degradation of the host matrix has made some

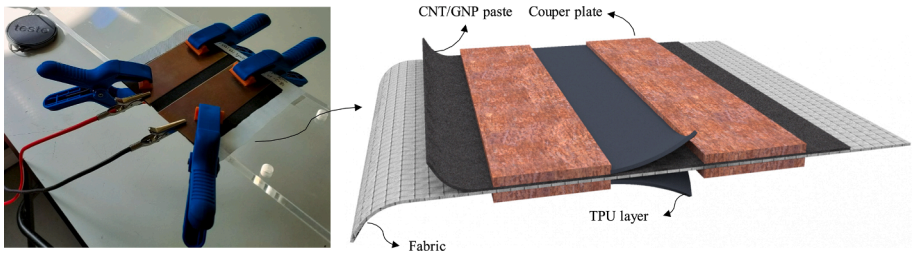


Fig. 8. The configuration of the test setup for electrical conductivity measurements and joule heating test.

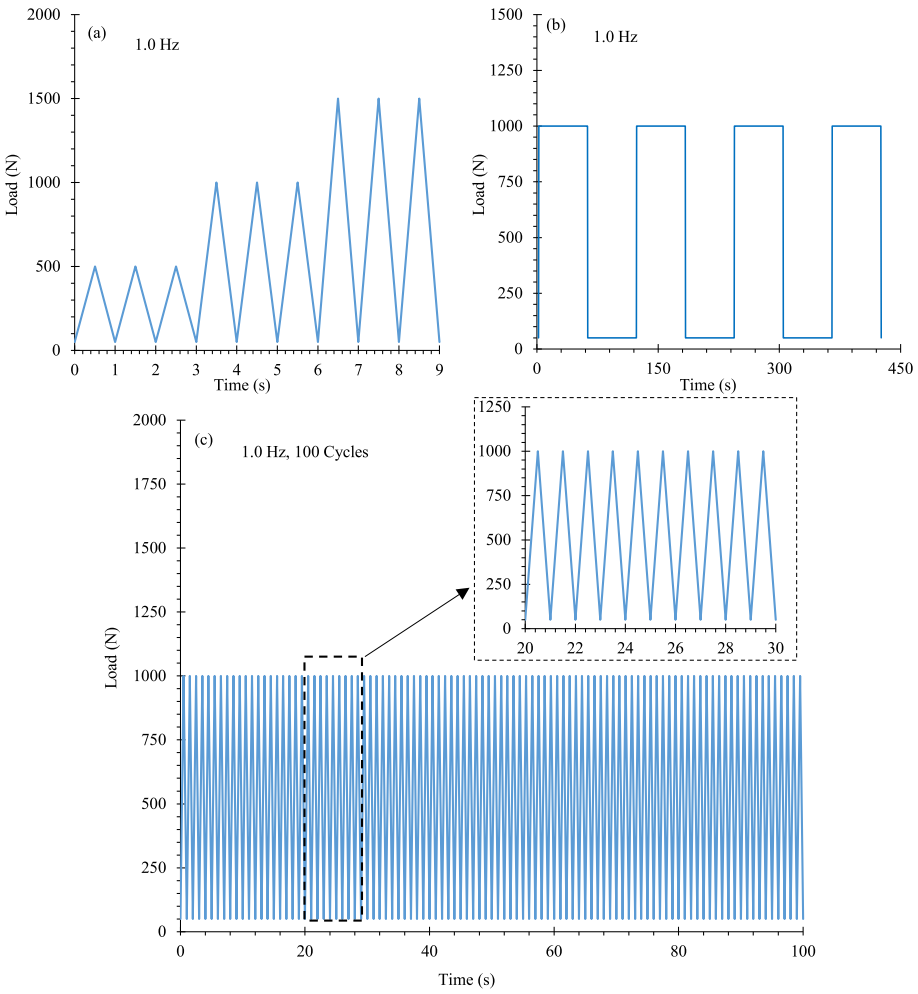


Fig. 9. Loading patterns used for the piezoresistivity investigation: a) multiple loading, b) creep loading, c) fatigue loading.

challenges for their wide implementation [8,31,32,37,38,42,43]. Furthermore, the incorporation of a high amount of phase-change materials or conductive filler to achieve the required heating performance may reduce the overall structural strength, which is not appropriate for long-term heavy loads [8,31,37]. However, some multifunctional materials and elements can both improve the mechanical properties of structures and carry out other advanced performances including heating, healing, sensing and monitoring [15,44–46]. This crucial role necessitates cost-effective materials with high durability, a simple production process and reliable and real-time sensing capabilities [6,7].

Braided composites including fibre-reinforced polymers (FRPs), 2D and 3D braided elements, various kinds of geosynthetics, braided bars and tubes, etc are common multifunctional and reinforcement materials employed in different structures [15,25,26,47–52]. Flexibility in production (woven, non-woven, synthetic, fibrous, natural), tailored mechanical properties, wide scope of geometry shapes (planar, grid, bar and tubular), adjustable permeability (high, moderate or none), and their compatibility with various structural elements and infrastructure, a wide range of durability, simple and fast production and implementation, and their cost-effectiveness, made these products particularly popular [6,52–59]. Jin et al. [52] introduced glass fiber textiles into the 3D printed cementitious composites and they report a significant enhancement in its toughness. Ventura et al. [51] reinforced the cement composite plates with nonwoven fabrics from technical textile waste fibres and found a high improvement in flexural strength and flexural strength (~15 MPa), fracture toughness (~3.5 kJ/m^2), and environmental impact of those panels. Murcia et al. [60] also reported an improvement in the flexural behaviour of thin polymer concrete panels reinforced with basalt fiber textile fabric.

Multifunctional or smart planar braided composites (SPCs) are also

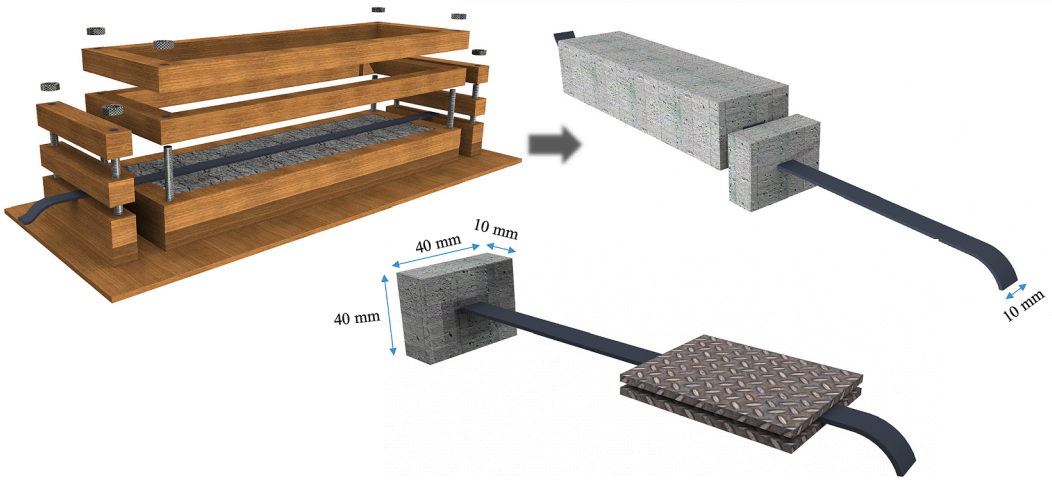


Fig. 10. Specimen configuration used for the pull-out test.

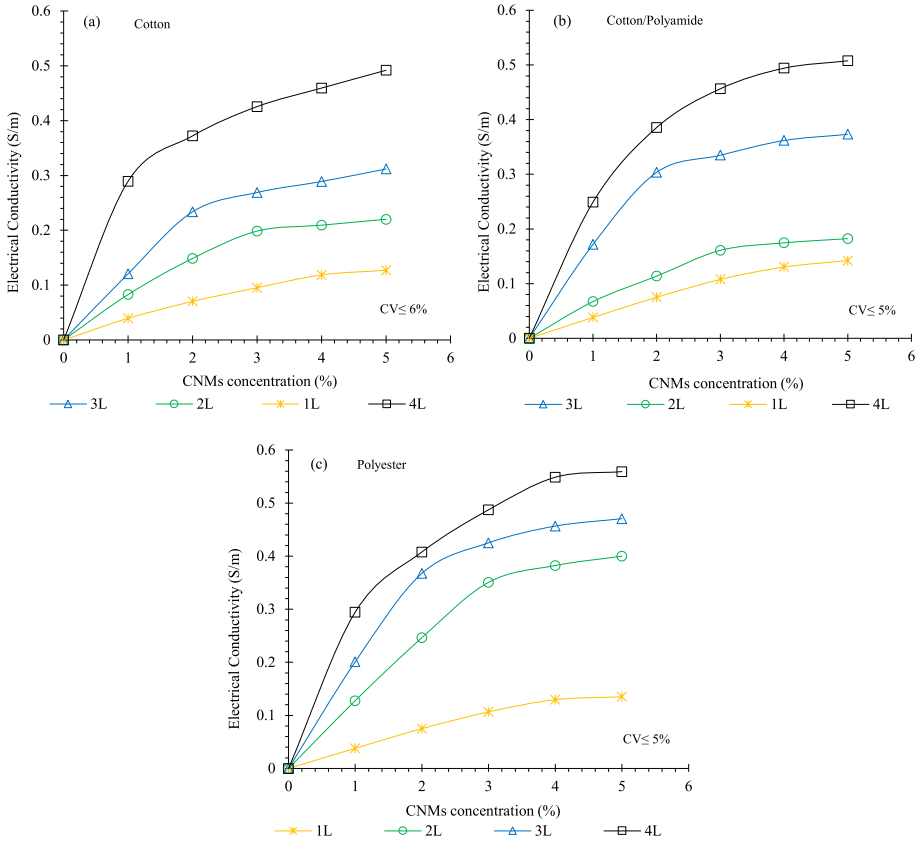


Fig. 11. Electrical conductivity of SPC, produced with different layers (1L to 4L) and CNMs concentrations: a) Cotton, b) cotton/polyamide, c) polyester.

capable of sensing stresses, strains, temperature, or other parameters by integrating them with sensors such as a stress meter or fibre optic [61,62]. Adhered strain gauges have been extensively employed as integrated sensing components with SPC over the past two decades, through several mounting techniques [63–65]. Rowe et al. [63] installed thirty-four strain gauges on the symmetry axis of a high-strength 360 × 210 cm polyester woven textile and used it for reinforcing and measuring the displacement of an embankment. However, they stated that the strain gauges were easily damaged. Gnanendran et al. [65] evaluated the stress in a fill slope using a polypropylene braided grid (870 × 740 mm) equipped with 12 pairs of foil strain gauges in different directions along the centreline. They found that using only one strain gauge per location markedly reduced the accuracy of the tensile strain and geogrid force estimated based on the nominal stiffness, particularly at low loads, and noted that considerable caution is required when utilising such an approach. Extensive studies regarding the development of SPC with embedded fibre optic sensors have also been conducted [66–68]. However, the implementation of these sensors requires a complex process otherwise the junctions are prone to slip, which may cause the embedded fibre optic to be stripped from the SPC [25]. The maximum strain of the fibre optic is roughly 10^{-3}, and its application in large deformation (such as the measurement of embankment or side slope) is restricted. Moreover, embedded fibre optics in SPC are prone to damage during field operations [26,69].

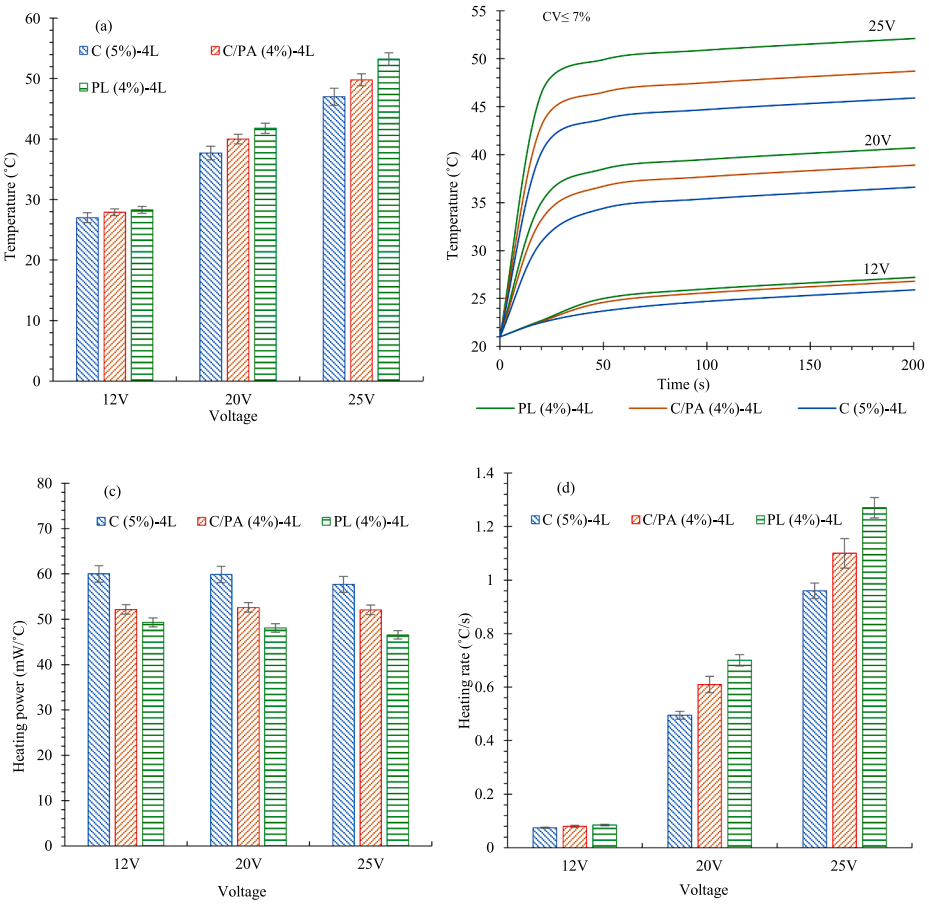


Fig. 12. Joule heating analysis: a) maximum temperature, b) heating trend, c) heating power, d) heating rates.

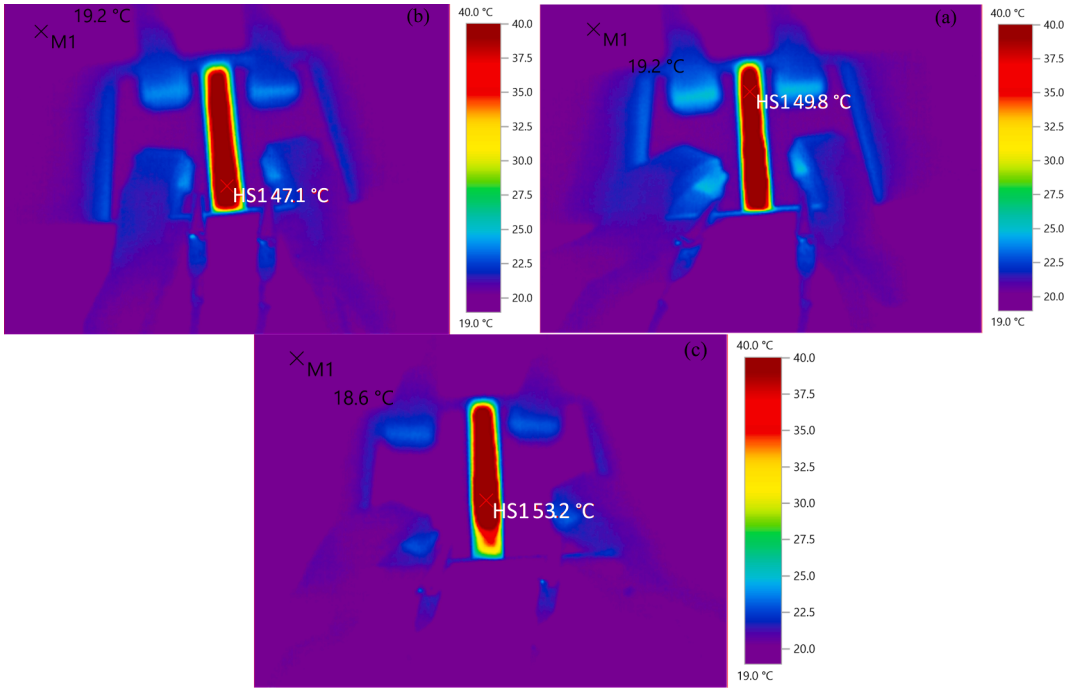


Fig. 13. Thermographic images of different smart elements: a) C (5%)-4L, b) C/PA (4%)-4L, c) PL (4%)-4L.

Table 5
Comparison of electrical conductivity and heating performances of different fabrics developed with different methods.

Fabric	Polymer/Solvent	Method	Nanoparticles	Composition	Conductivity	Voltage (V)	Temp (C)	Time (s)	Ref
Cotton	Polyurethane based resins	Screen Printing	GNPs,	12 w/v %	$(9.39 \pm 1.28 \times 10^{-1})$ S/m	12	40.4	300	[98]
Cotton	Polyurethane based resins	Screen Printing	GNPs + CNTs	5 w/v %	$(9.02 \pm 6.62 \times 10^{-2})$ S/m	12	42.7	300	[98]
Cotton	Water	Dip-dry	SWCNTs	0.1 wt%	–	20	90	20	[109]
Cotton	Water	Dipping drying	Functionalised MCWNTS	1.0 wt%	–	60	80	300	[110]
Cotton	PEDOT: PSS	Dip-coated and coating	Reduced GO	3.2 mg/m^2	–	30	70.5	30	[111]
Cotton	Deionized water	coating	GNPs and carbon black particles	1 wt%	–	50	97.2	600	[112]
Wool	Deionized water	coating	GNPs and carbon black particles	1 wt%	–	30	93.4	600	[112]
Cotton	Waterborne Polyurethane	Pad-dry-cure	GNPs	480 mg/m^2	–	–	100	658	[113]
Cotton	Thermoplastic polyurethane	Impregnation	GNPs	5 wt%	(10^{-4}) S/m	–	–	–	[105]
Cotton	Thermoplastic polyurethane	Impregnation	GNPs	30–40 wt%	(1.0×10^{3}) S/m	–	–	–	[105]
Cotton	Polypyrole	Impregnation	GNPs	2:1 wt%	1.703 S/cm	–	–	–	[104]
Flax	Polypyrole	Impregnation	GNPs	2:1 wt%	0.289 S/cm	–	–	–	[104]
Wool	–	Impregnation	GNPs + carbon black	2:1 wt%	0.686 S/cm	–	–	–	[104]
Flax	Chitosan	Dip-pad-dry	GNPs	2 wt%	(4.0×10^{-1}) S/m	–	–	–	[114]

Self-sensing SPCs are a piezoresistive kind of composite with intrinsic sensing capabilities that can provide an integrated, real-time, and practical solution for different infrastructural monitoring [70,71]. Generally, in a piezoresistive composite, the effects of external factors such as stress, strain, and temperature can be detected by measuring the fractional change in electrical resistivity [23,72,73]. Self-sensing SPCs are generated with conductive fibres or polymers using different processes including knitting, coating, and 3D printing [25,74–77]. Conductive polymers are generally composed of different conductive fillers such as carbon nanomaterials (CNMs) [78–80]. Abedi et al. [15] used self-sensing braided composite rods developed by carbon nanomaterials and epoxy resin, as reinforcement and strain detection of the concrete beams. Zhang et al. [48] used a fibrous composite laminate composed of epoxy resin and carbon fibers for in-situ damage sensing in structural elements. They employed a spray coating technique to deposit carbon nanotubes onto carbon fibre prepregs. However, the planar fibrous composites showed low interlaminar toughness due to the brittle nature of most epoxy matrices [48,81]. A graphene oxide-coated textile was developed by Irfan et al. [21] for stress and strain detection in the cementitious composite. Cui et al. [75] recently studied the piezoresistivity behaviour of the grids doped with conductive polymers. In addition to reinforcing the structures, these grids can function as self-monitoring systems. Hatami et al. [44,74] studied the strain sensitivity and piezoresistivity response of polyvinylchloride/carbon black (PVC/CB) composites to cyclic tensile loading in order to develop smart geogrids. As a result of cyclic deformation, the conductive network in the coating specimens filled with higher-structure CB showed less damage and more recovery in tensoresistivity. Li et al. [26] developed a piezoresistive geobelt which is made of high-density polyethylene filled with carbon black using a twin extrusion. However, they used a wire as the electrode in the loading region which may reduce the reliability of the results due to the contribution of the electrode effects. Furthermore, despite these advances, there are no effective methods to resolve the influence of surrounding environmental factors particularly moisture on the conductivity and piezoresistivity behaviour of the SPCs, while it is one of the most interfering parameters in civil projects.

Furthermore, to the best of the authors' knowledge, there are no extensive studies regarding benefiting the heating generation of SPCs in cementitious composites. However, much effort and progress have been made to develop self-heating wearable braided composites [82–85].

Therefore, developing a multifunctional planar braided composite with capabilities of reinforcing, self-sensing and self-heating simultaneously, for large-scale field applications in civil engineering is still facing challenges. In this paper, in order to address this issue and bridge the existing knowledge an integrated SPC was developed through coatings on different host fabrics including Polyester, Cotton/Polyamide, and Cotton. In this route, various concentrations of hybrid carbon nanotubes (CNT) and graphene nanoplatelets (GNP) were dispersed with a specific technique, into a combination of polyurethane-based polymeric resins. The conductive polymeric paste was then applied to the surface of the fabrics using the screen printing method, in numerous layers. The optimized samples in terms of electrical conductivity were sealed by a waterproof thermoplastic polyurethane resin using the knife coating technique. Self-heating (Joule heating) performance of the samples was then measured using different voltages. The surficial and microstructural status of the samples were assessed using different tests. The produced samples were subsequently placed in a cementitious mortar. Finally, the mechanical, self-sensing, and self-heating performances of the specimens were investigated.

The outcomes of this study provide insight into the development of new multifunctional braided composites including reinforcement and geosynthetics, with several applications in civil engineering.

2. Experimental campaign

2.1. Raw materials

Carbon-based nanomaterials GNPs and multiwall carbon nanotubes (MCWNTs) were obtained from Graphenest in Portugal and Iolitech Ionic Technologies, Germany respectively. The X-ray spectra, morphology and characteristics of GNPs and MWCNTs used in the study are shown in Fig. 1, Fig. 2 and Table 1 respectively. Polyurethane-based resins that are commercially available as Edolan CM and Tanapur Velutho, used in this study, were acquired from Tanatex Chemicals based in the Netherlands. Thickener A 02 was also brought from the same company. The physical properties of the resin and thickener are presented in Table 2. The cotton, polyester and cotton/polyamide fabrics were purchased from Lameirinho, Portugal. The physical and mechanical properties are displayed in Table 3 and additionally, the morphology of the fabrics is exhibited in Fig. 3. Thermoplastic polyurethane (TPU) was obtained from TRINSEO in the form of pellets. Solvents such as N, N – Dimethylformamide (DMF) were acquired from Sigma Aldrich, Germany and Tetrahydrofuran (THF) from Fischer Chemicals, UK. In this study an ordinary Portland cement type I (CEM I

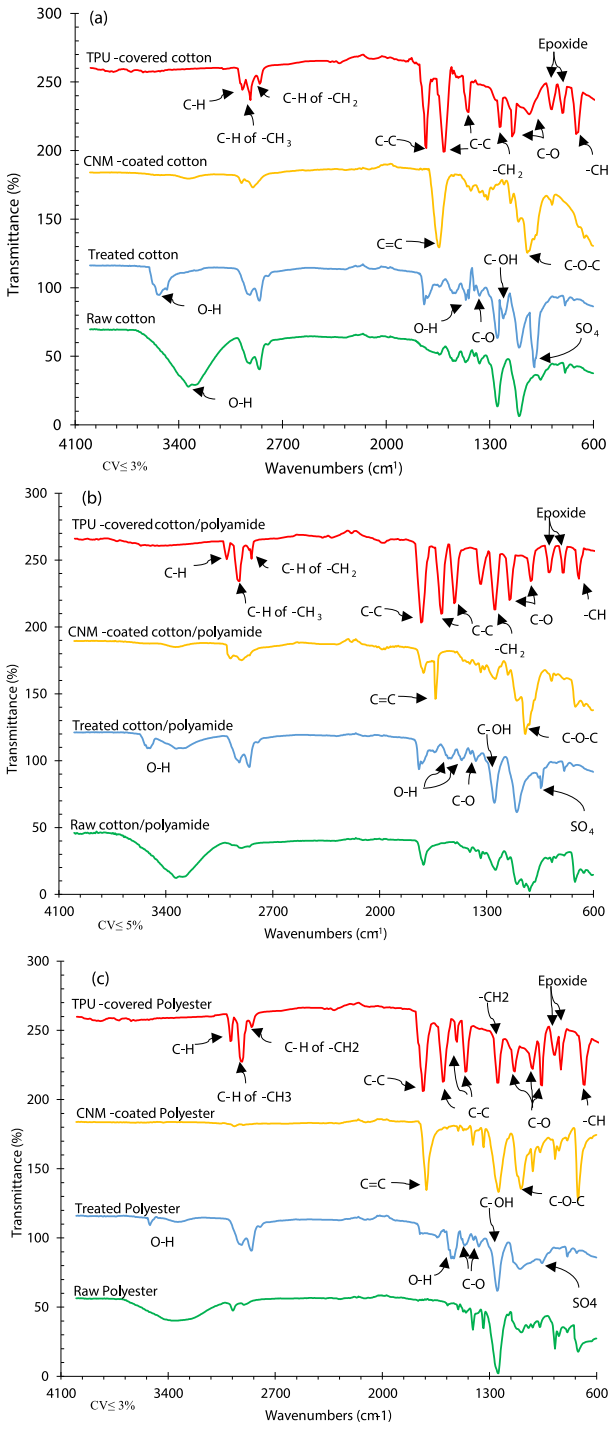


Fig. 14. FTIR spectra of: a) cotton, b) cotton/polyamide, c) polyester.

42.5R) and standard sand (EN 196-1) with siliceous and clean particles were used [86,87]. The particle size distribution of the cement and sand and their main physical characteristics are presented in Fig. 4 and Table 4.

2.2. Smart fabric composite development and characterization methods

2.2.1. Carbon Nano materials (CNMs) dispersion

In this study, equal portions of Edolan/Tanapur (1:1) were used as host resin for conductive paste production. The proper dispersion of CNMs into the paste is a requirement to maintain their distinctive features [88,89]. Indeed, the high viscosity of the polymers, the presence of strong surface van der Waals forces between CNMs, and their high specific surface area and aspect ratio cause a high tendency of CNMs to form agglomeration [90–92]. Hence, an effective dispersion method is required to take advantage of the unique properties of the nanoparticles.

In this route, the required concentration of the CNTs/GNPs (1:1) was added to the acetone (1:2 of the host resin). The solution was stirred using a magnetic stirrer at 800 rpm/min for 1 h. The solution was then placed into a 45 kHz bath sonication to exfoliate the CNMs bundles and agglomerations. Edolan/Tanapur was added to the solution after 1 h of sonication. The suspension was then mixed using a high-speed mixture for 14 h to complete the evaporation of acetone. Before the printing process, the thickener (approximately 0.07% w/v) was added to the paste and mixed for 30 min. A schema of the paste production process is shown in Fig. 5.

2.2.2. Fabrics coating method

In this paper, a chemical surface modification for the fabrics was used to improve the conductive polymer paste deposition on the surface of the fabrics. For this purpose, the raw fabrics were immersed in diluted sulfuric acid (H_2SO_4) solutions at room temperature in a bath ratio of 1:40 for 15 min. The concentrations of H_2SO_4 aqueous solutions ranged from 2 g L^{-1} to 25 g L^{-1}. The treated samples were then cured at 110 °C for 6 min in a heat-setting machine. The CNT/GNP conductive paste was then coated on the fabric substrate using the screen-printing method. The samples were coated with 1, 2, 3, and 4 layers for 1%, 2%, 3%, 4%, and 5% of CNT/GNP (w/v) concentration using screen printing. A Johannes Zimmer (Austria) semi-automatic printing machine with a polyester screen (Weft density = 34/cm^2, Warp density = 31/cm^2) was used to perform the screen-printing process. The sample was then dried (Mathis AG, Oberhasli and Switzerland) for 3 min at 120 °C after each layer printing and finally cured for 3 min at 160 °C (Ramola Bruckner). A schema of the coating process is illustrated in Fig. 6.

In this study, TPU polymer was used as a protective and waterproof layer due to its high toughness, flexibility and tear resistance, low cost, good adhesion, resistance to chemical agents, and hydrophobic properties [93–95]. The TPU polymer was prepared by mixing the solvents DMF and THF in a ratio of 2:1. TPU pellets were added to the solvents in such a way that it has 30 % (w/w) concentration and the solution was subjected to magnetic stirring for about 60 min by maintaining the temperature of 40 °C [96]. The polymer was applied using ZAA 2300 automatic film applicator from Proceq. The sample was fixed on the table and proper masking was done. The applicator was positioned on the sample before placing the polymer in front. The applicator was then operated by selecting the forward option on the machine and a layer was coated.

2.2.3. Cementitious composite casting and reinforcing

In this study, cement mortar was used as the host cementitious composite. Specific moulds were produced by a 3D printer and used for specimen fabrication as shown in Fig. 7. For the specimens to be used in self-sensing and self-heating tests, the SPC samples were printed in a rectangular shape with a blank space in the middle to improve the sensing, heating and mechanical performance. Cementitious mortar was prepared following EN 196–1:2016 standard. First, a sufficient amount of mortar was poured into the moulds, then the SPC samples were placed and fixed at a distance of 1 cm from the bottom of the moulds, then the rest of the mortar was poured into the moulds in three steps and vibrated using a table. The specimens were demoulded after 24 h and cured for 28 days according to the standard.

2.2.4. Electrical conductivity measurement

The electrical conductivity was measured by using equation (1). For this purpose, the resistance needs to be measured by using a Keithley 487 Picoammeter/Voltage source. The setup consists of four copper plates placed at a distance of 1 cm and the plates were connected to the voltage source via crocodile cables as shown in Fig. 8. The clamps were

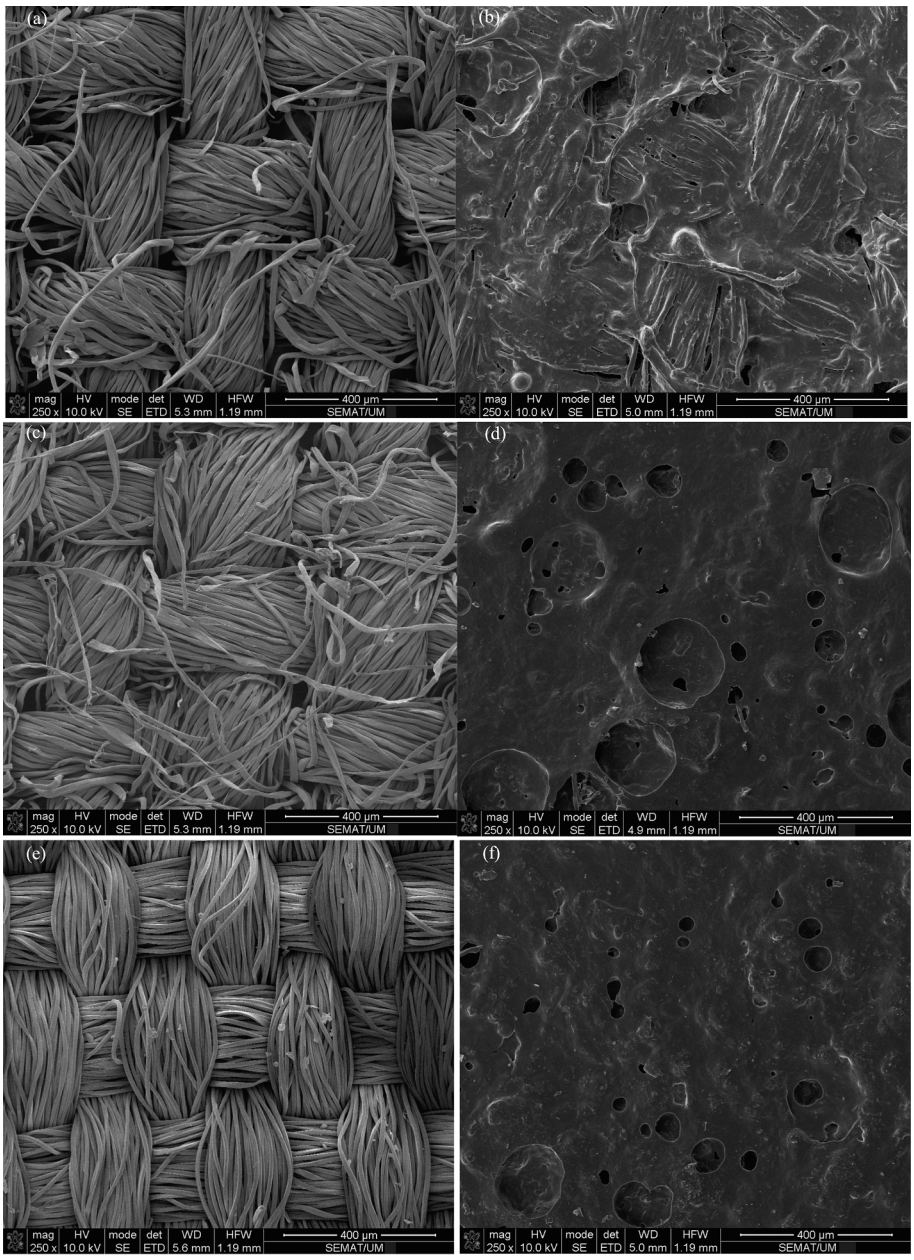


Fig. 15. SEM morphology of a) raw cotton, b) CNM-coated cotton (without TPU), c) raw cotton/polyamide, d) CNM-coated cotton/polyamide, e) raw polyester, f) CNM-coated polyester.

used to hold the copper plates in their respective place. A voltage of −0.8 V to 0.8 V was sent across the sample with a step of 0.1 V and a graph was drawn between the voltage and the current. The test was repeated 5 times and the average values were used to draw the graph. The slope of the graph gives the resistance of the sample and by using Eq. (1) the resistivity in *Ωm* was calculated. The electrical conductivity (S/m) of the sample will be the inverse of the resistivity [97].

$$\rho = R \times \frac{A}{L}(\Omega m) \tag{1}$$

where ρ is resistivity (Ωm), R is resistance (Ω), A is cross-sectional area (m^2), and L is the distance between the electrodes (m).

2.2.5. Joule heating (self-heating) investigation

A thermal Imager (Testo 885), a CPX200 D Dual 180 Watt DC power supply from Power Flex, copper plates, clamps, crocodile cables and acrylic were used to measure the joule heating of the samples. The samples were fixed in between the copper plates with the help of clamps. The crocodile cables were used to connect the copper plates and the power supply. Required voltages were sent across the sample and the temperatures attained on the surface of the samples were observed via thermal imager and recorded at various time intervals [98]. The heating power was calculated by using Eq. (2).

$$P = \frac{VI}{(T_0 - T_{max})} \tag{2}$$

where P is power, V is voltage (V), I is current (A), T_0 is room temperature (℃), and T_{max} is the maximum temperature (℃).

2.2.6. Piezoresistivity (self-sensing) assessment

In this study, the two probes technique (Fig. 7) was used for the evaluation of fractional changes in the electrical resistivity (FCR) of SPC-reinforced cementitious composite subjected to cyclic axial flexural loading. A digital multimeter (Aligent 34461a) was connected to the rest

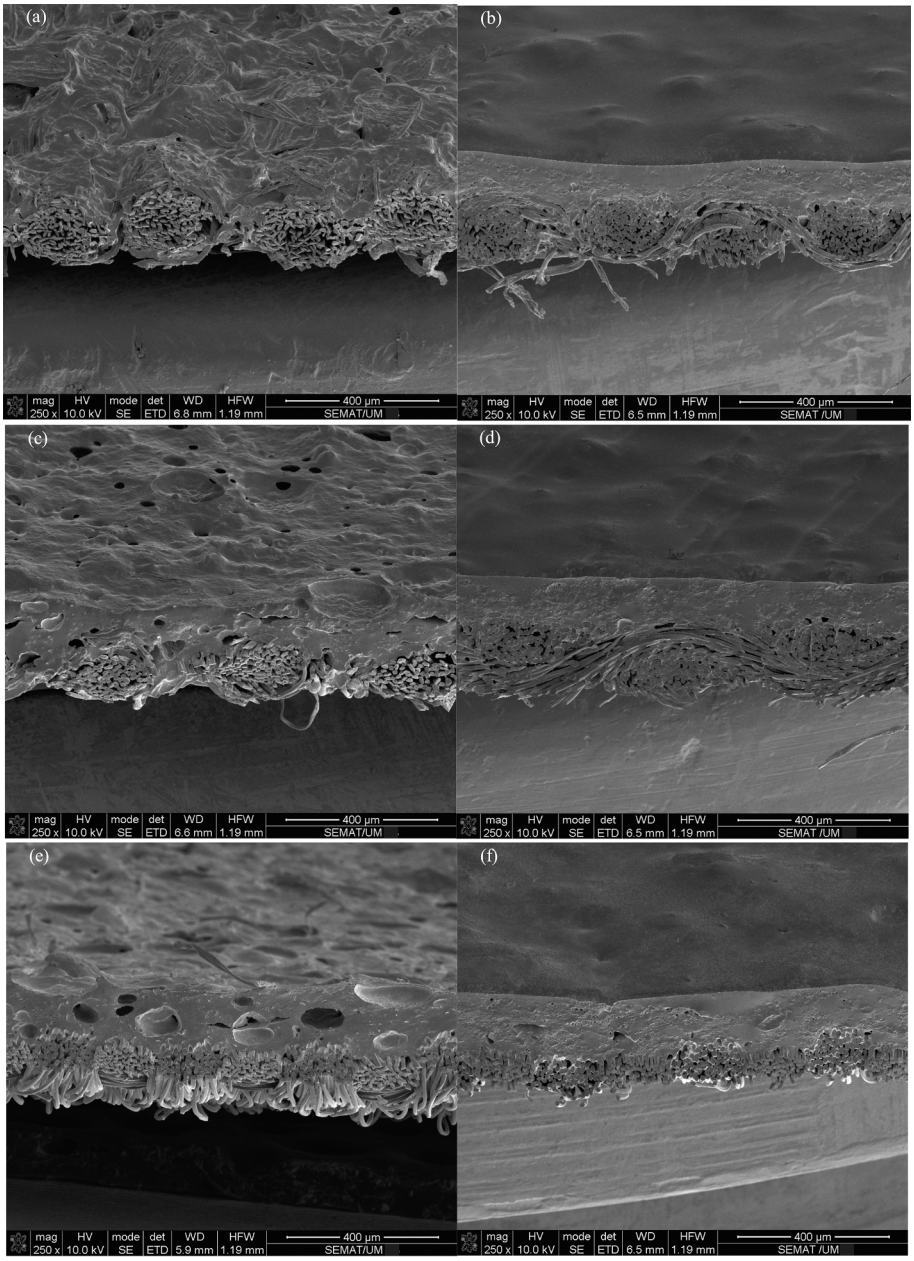


Fig. 16. SEM morphology of: a) CNM-coated cotton, b) TPU-covered cotton, c) CNM-coated cotton/polyamide, d) TPU-covered cotton/polyamide, e) CNM-coated polyester, f) TPU-covered polyester.

part of the SPCs, out of the specimen. Alligator clamps were fixed on the sample using copper sheets and conductive glue. Cyclic flexural loading (Fig. 9) with different shapes and magnitudes with 1.0 Hz speed was used for self-sensing assessments. The FCR was calculated using equation (3) for the following investigation of piezoresistivity behaviour:

$$FCR = \frac{\rho_{(t)} - \rho_0}{\rho_0} \tag{3}$$

where $\rho_{(t)}$ is the resistivity at the time (t) during the test and ρ_0 is the initial electrical resistivity, which is measured before loading. The sensitivity of SPC-reinforced cementitious composite against the strain was also measured by the gauge factor (GF), defined as the relative change in electrical resistivity over the strain, given by equation (4):

$$GF = \frac{FCR}{\varepsilon} \tag{4}$$

where ε is the applied flexural strain at bottom of the cementitious specimen.

2.2.7. *Mechanical and microstructural investigation*

The flexural strength of the SPC-reinforced cementitious composite was assessed following EN 196-1:2016 standard. The results were calculated as the mean of the values obtained for at least three specimens. The tensile strength of the fabrics was also evaluated using MTS Exceed E45 according to ISO 13934-1:2013. Furthermore, the morphology surfaces of the fabrics after printing and also coating with the TPU were investigated using scanning electron microscopy. It is one of the effective methods for microanalysis and failure analysis of solid inorganic materials [99-101]. For this purpose, the surface of the sample was first cleaned and coated with 30 nm of Au–Pd thin film using a high-resolution sputter coater (Cressington 208HR). During the analysis a Nano SEM NOVA 200, FEI/SEM-FEG microscope was employed in the secondary electron mode at an acceleration voltage of 10 kV.

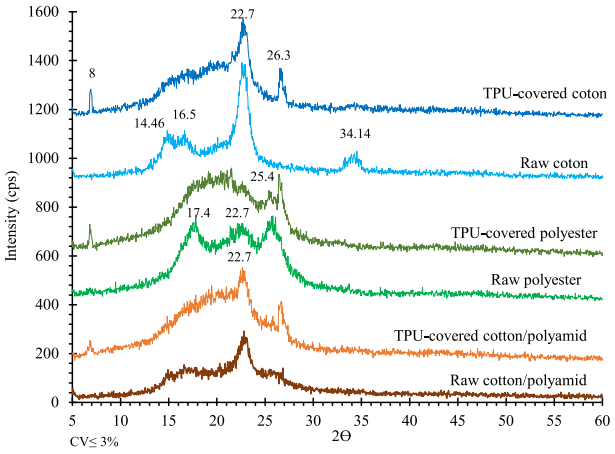


Fig. 17. XRD analysis of raw, CNM-coated and TPU-covered fabrics.

Thermogravimetric analysis (TGA) of the samples was also conducted to assess the thermal stability of the samples and their ingredients using an SDT-2960 instrument at a maximum temperature of up to 600 °C and a heating rate of 10 °C min^{-1} in a nitrogen atmosphere (flow rate 100 mL min^{-1}).

In order to analyze physical properties such as phase composition and crystallographic structure of the samples, X-ray diffraction analysis (XRD) was also conducted. The XRD analyses were done on a Bruker AXS D8 Discover diffractometer equipped with Cu-Kα radiation (λ = 1.54060 Å) at 40 kV and 40 mA, using a Locked Coupled configuration. The diffraction patterns were acquired between 5° and 60° with a step size of 0.04° s^{-1}. In addition, Fourier transforms infrared spectroscopy (FTIR) was done to identify chemical bonds and surface analysis of the fabrics after treatment and coating. FTIR spectra were recorded on a Shimadzu IRAffinity-1S spectrometer. The spectra were acquired in the range of 4000–600 cm^{-1} at a nominal resolution of 16 cm^{-1}.

2.2.8. Pull-out test

A single-strip pull-out test was performed to investigate the interfacial properties of the SPC-cement matrix. In this route, a single stripe of the SPC was placed at the centre of the cementitious mortar along the specimen length using similar moulds to section 2.2.3 (Fig. 10). Each specimen was cut to 10 mm thickness. The theoretical embedded length of the strips was calculated based on the lowest bond strengths for the successful pull-out of the SPC without rupture [102,103]. During the test, the pull-out speed was constantly controlled to a displacement rate of 0.02 mm/s and the average shear bond strength, τ_{max}, was calculated using equation 5 [13,102]:

$$\tau_{max} = \frac{P_{max}}{2L(b+t)}$$

where P_{max} is the maximum pull-out load, L is the embedded length, and b and t are the width and thickness of the strip respectively.

3. Results and discussion

3.1. Electrical conductivity

The influence of CNMs percentages, the number of printed layers, and the nature of the fabrics on the electrical conductivity are presented in Fig. 11. As mentioned previously, the fabrics are coated with 1 to 4 layers and the paste used for coating was produced with different CNMs concentrations in the range of 0 to 5 % to achieve the required conductivity and joule heating performances [98,104,105]. As shown in Fig. 11 the electrical conductivity of all the fabrics improved with the increasing CNMs concentration. The results indicated a similar trend for electrical conductivity enhancement influenced by increasing the number of printed layers in samples. Increasing the CNMs concentration and number of printed layers, caused an increase in conductive path formation and consequently improve the electrical conductivity.

The hybrid CNT/GNP dispersed into the polymeric resin, with one and two-dimensional geometry shapes (Fig. 2), facilitates the formation of conductive paths by improving percolation and tunnelling effects [7].

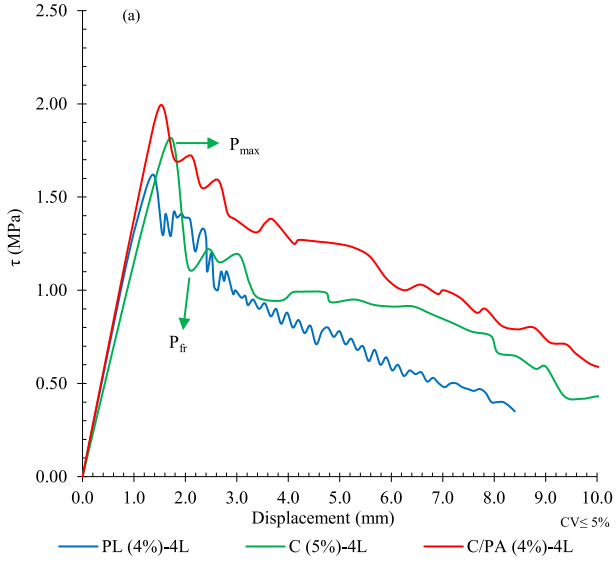


Fig. 19. Average shear bond strength for different SPC along the pull-out test.

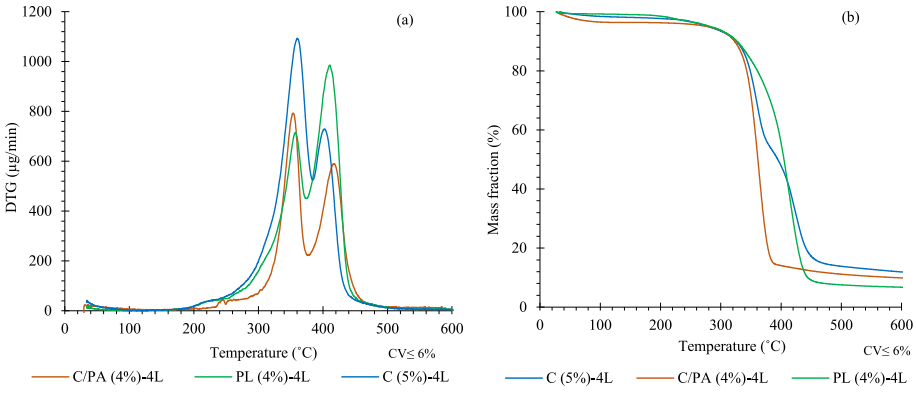


Fig. 18. Thermography analysis of the fabrics: a) DTG diagrams for different smart fabrics, and b) TGA diagrams for different smart fabrics.

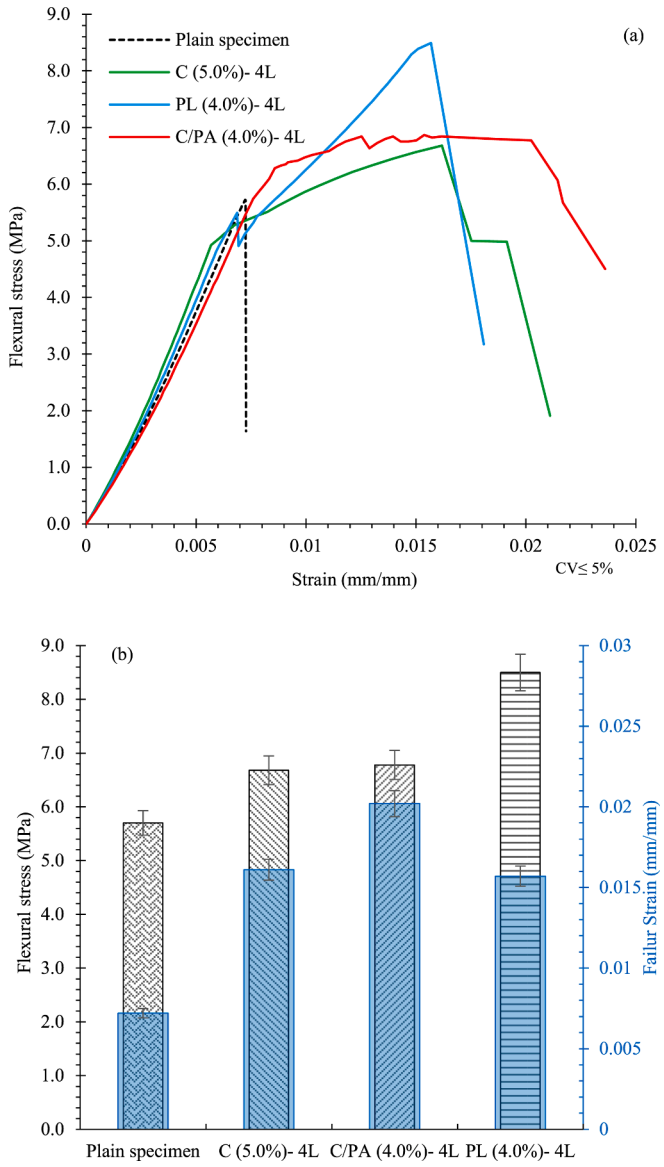


Fig. 20. Main mechanical properties of cementitious composite reinforced with different smart elements: a) stress/strain curves and b) maximum flexural strength vs failure strain.

The "percolation threshold" is the critical concentration of a conductive phase at which a composite can undergo a transition from an insulator to a conductor. Indeed, increasing the conductive phase concentration beyond of percolation threshold might not increase the conductivity of the composite significantly [5,91].

As can be observed in Fig. 11, increasing the number of printed layers reduced the percolation threshold concentration. For all types of fabrics, in the samples printed with one layer, the percolation threshold was around 4.0%. However, the threshold concentration in the samples printed with 2, 3, and 4 layers was reduced to 3, 2, and 1.0% respectively. Hence, it can understand that the percolation threshold can be reached with low concentrations when more layers of printing are performed. Additionally, the number of layers has more influence on electrical conductivity rather than the concentration of the CNMs.

An increase in the number of layers will increase the thickness of the coating which results in the improvement of the conductive path and a sharp increase in electrical conductivity, while an excessive increase in the thickness can reduce the volume of electrical conductivity of the sample (Eq. (1). However, the initial layers of print might be utilized to fill the voids of the fabric texture and have no significant effect on increasing the thickness of the sample.

In cotton samples, increasing the printing layers' number from 1 to 2, 3 and then 4, caused an increase in electrical conductivity of the samples covered with 1.0% CNMs by approximately 1, 2, and 6 times respectively. These amounts for cotton/polyamide and polyester samples were around 0.7, 3.5, and 5.5 and 2, 4, and 6 times. Generally, the electrical conductivity of the polyester samples was higher than cotton/polyamide and cotton samples coated with an equal CNMs percentage and printing layers' number. Indeed the cellulose acts as an insulator [98] and hence, the electrical conductivity is lower for cotton than the cotton/polyamide and polyester samples.

Based on the above results, the smart element composed of cotton fabrics coated with 4 layers of the conductive paste containing 5.0% of CNMs and the smart elements composed of cotton/polyamide and polyester fabrics coated with 4 layers of the conductive paste containing 4.0% of CNMs, was selected as optimum samples to perform the further assessment. These samples were identified with C (5.0%)- 4L, C/PA (4.0%)- 4L, and PL (4.0%)- 4L respectively.

3.2. *Self-heating performance*

The joule heating was performed for various samples at several voltages (12 V, 20 V, 25 V) and the temperatures attained are shown in Fig. 12. The highest electrical conductivities were observed for the samples coated with more layers of the conductive paste. Hence, those samples were subjected to the joule heating tests. It was observed that cotton has attained lower temperatures in comparison with the other two types of fabrics (polyester and cotton/polyamide) and polyester has achieved the highest temperatures. The samples with the highest electrical conductivity have shown the highest temperatures on their surface. Similar observations were observed in a previous work of the authors [98]. The lowest electrical conductivity of the cotton can be attributed to the presence of cellulose in cotton [106], which acts as an electrical insulator [107,108] As polyester is a non-cellulosic fibre, the electrical conductivity was higher in comparison with other samples. The increment of the surface temperatures of the samples is shown in Fig. 12 b and it is observed that all samples have shown an increment in temperatures in the first 20 s and thereon, temperatures stabilize. The temperatures were increased with an increase in voltage and the highest temperature (approximately 53 ℃) was achieved for the polyester sample with 4 layers when 25 V was supplied followed by cotton/polyamide (approximately 49 ℃) and cotton (approximately 47 ℃). Indeed Joule heating is caused by interactions between the body of the conductor and charge carriers (usually electrons). An electric field is created with a potential difference (voltage) between two points of a conductor. The electric field accelerates charge carriers in the direction of the electric field, providing them with kinetic energy. In the conductor body, charged particles collide with quasiparticles (canonically quantized, ionic lattice oscillations in the harmonic approximation of a crystal), which transfer energy from electrons to the lattice by generating further lattice oscillations. Indeed, the oscillations of the ions are the origin of the thermal energy (radiation) measured during a typical experiment. Increasing the voltage rises the kinetic energy of the charge carriers and consequently increases the thermal energy. From Fig. 12 c, it can be observed that less power is required for the polyester sample when compared to others. This is in agreement with the results from the electrical conductivity, where the sample with higher conductivity can get heated with less power. Additionally, from Fig. 12 d, it can be noted that the polyester sample has a higher heating rate compared to the other two samples. It can be concluded that the heat rate raise was higher for the samples which have high electrical conductivity. As mentioned before, the good connection between the carbon nanoparticles and the absence of cellulosic materials has contributed to a higher heating effect for polyester samples. Fig. 13 shows the images of the samples observed with the thermal images where the surface

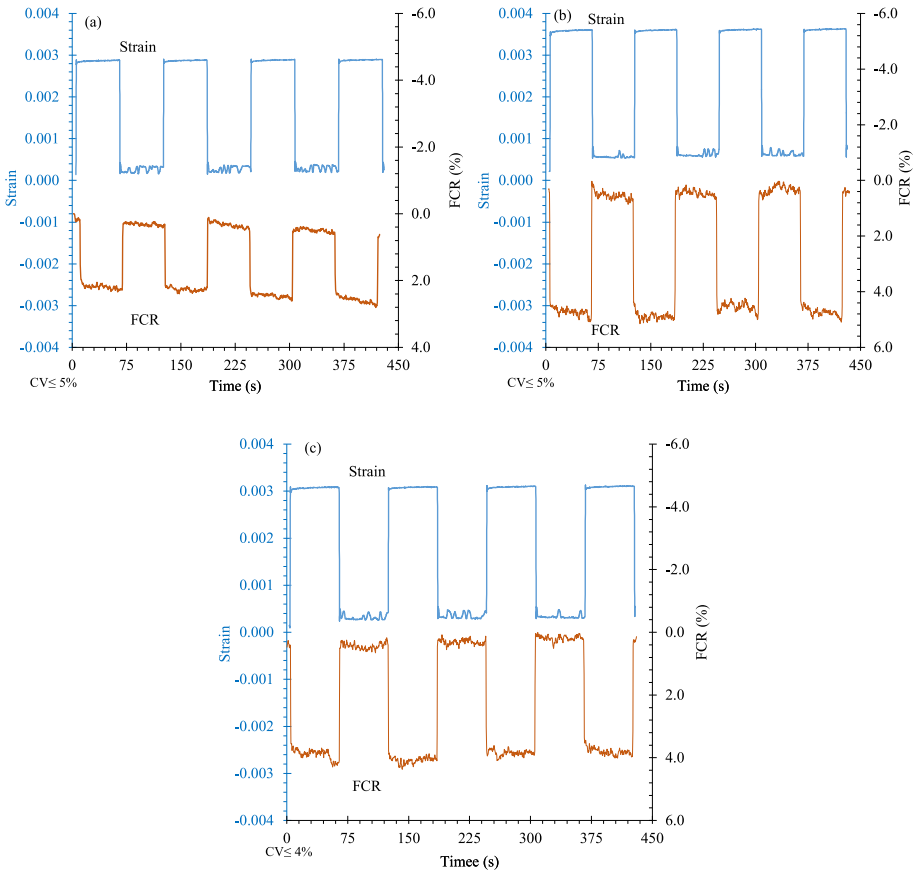


Fig. 21. Piezoresistive responses of the cementitious composites reinforced with different smart elements under creep flexural cyclic loading: a) C (5.0%)- 4L, b) C/PA (4.0%)- 4L, C) PL (4.0%)- 4L.

temperature of the samples was measured. It can be noted that the polyester sample with 4 layers has achieved a temperature of 53.2 ℃.

A comparison of electrical conductivity and heating performances of different fabrics developed with different methods in prior studies is presented in Table 5.

3.3. *Fabrics' surficial and microstructural characterizations*

Fig. 14 shows the FTIR spectra of raw, modified, CNMs-coated and TPU-covered samples of cotton, cotton/polyamide, and polyester fabrics. The typical bands of cellulose, lignin and hemicellulose were observed. The strong peak of the hydroxyl (OH) groups of cellulose, lignin and water was observed at 3330 cm^{-1} for the raw fabrics [115]. The peak at 2920 and 2854 cm^{-1} in raw cotton, and 2897 cm^{-1} in raw cotton/polyamide were assigned to bending and stretching vibrations of C-H present in cellulose and hemicellulose, while the strong peak at 2904 and 2896 cm^{-1} in raw polyester corresponded to the C-H stretching vibration of the benzene ring and the skeletal vibration of the aromatic systems in the polyester chains [116,117]. The band at 1639 and 1622 cm^{-1} in raw cotton and cotton/polyamide might be related to the presence of water in the fabrics [118]. The absorption band at 1462 cm^{-1} in raw cotton, 1477 cm^{-1} in raw cotton/polyamide, and 1338 and 1345 cm^{-1} in raw polyester was associated with the CH_2 symmetric bending of the cellulose [119,120]. A peak at 1409 cm^{-1} corresponded to aromatic C-C stretching and C-H in-plane bending, of raw polyester spectra [120]. The observed peaks at 1369 and 1315 cm^{-1} in raw cotton were assigned to bending vibrations of the C-H and C-O groups of the aromatic rings in cellulose polysaccharides, respectively [119]. The peaks at 1242 and 1094 cm^{-1} in raw cotton, 1244 and 1103 cm^{-1} in cotton/polyamide, and 1246 and 1091 cm^{-1} were assigned to C-O vibration. The peak at 1049 cm^{-1} in raw cotton/polyamide and 1045 cm^{-1} in raw polyester was due to aromatic =C–O and (OH) stretching vibrations of the polysaccharide in cellulose [119,120]. A peak at 1504 cm^{-1} in raw polyester was also characteristic of the benzene ring vibration [120]. The peak at 794 cm^{-1} in cotton, 867 and 721 cm^{-1} in raw cotton/polyamide, and 871, 844, and 794 cm^{-1} in raw polyester indicate the presence of β-glycosidic linkages between monosaccharides [121,122].

These peaks of the modified sample became stronger or eliminated compared with those of the original sample because the treatment with dilute H_2SO_4 solution increased bound water and/or caused the formation of functional groups (e.g. oxygen functional groups) on the surface of the fabrics [120]. The peaks at 1625 cm^{-1} in the treated fabrics might be attributed to the bond stretching of C–OH oxygen functional groups due to the reaction of H_2SO_4 and lignin which was more intense in treated cotton/polyamide and polyester. The new peaks at 1002, 945, and 952 cm^{-1} of the modified cotton, cotton/polyamide, and polyester samples corresponded to the C-S and S-O stretching of SO_4^{2} functional groups. Generally, the results indicated well the introduction of the functional groups into the fabric's macromolecules.

It is known that the existence of functional and polar groups improves the hydrophilicity of the fabrics and the adhesion of the host polymer [120]. In CNMs-coated samples, the new strong peaks at 1643, 1640, and 1712 cm^{-1} corresponded to double bonds C=C stretching of aromatic rings in CNTs and GNPs. The band at 1045 cm^{-1} in CNM-coated cotton and cotton/polyamide and 1095 cm^{-1} in CNM-coated polyester was the characteristic absorption of C–O–C stretching vibrations in esters and ethers of the host polymer constituent.

The characteristic peaks of the TPU-covered fabrics were almost the same. The bands were assigned as follows. The symmetrical and asymmetrical C-H stretch in aromatics caused a light peak at 2995 cm^{-1}. The peak at 2916 cm^{-1} was related to the asymmetrical C–H stretch of the

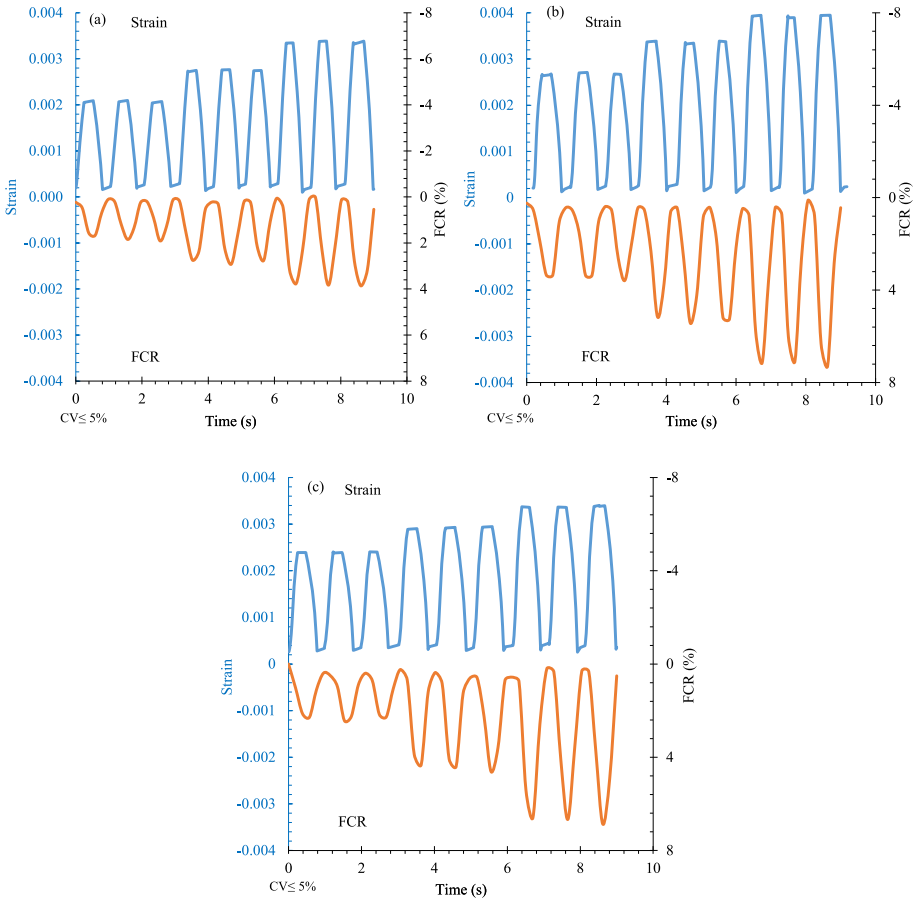


Fig. 22. Piezoresistive responses of the cementitious composites reinforced with different smart elements under multiple flexural cyclic loading: a) C (5.0%)- 4L, b) C/PA (4.0%)- 4L, C) PL (4.0%)- 4L.

–CH_2 group. The symmetrical and asymmetrical C–H stretch of the –CH_3 group caused also a peak at 2848 and 2965 cm^{-1} respectively. The peaks at 1735, 1595, 1519, and 1458 cm^{-1} corresponded to C–C stretching vibration in aromatic. The peak at 1242 cm^{-1} was related to the asymmetrical –CH_2 deformation. The peak at 1245 cm^{-1} was assigned to the asymmetrical aromatic C-O stretch. The peaks at 1185 and 1034 cm^{-1} were attributed to the asymmetrical aliphatic and symmetrical aromatic C-O stretch respectively. The –CH out-of-plane deformation in aromatic also caused a strong peak at 678 cm^{-1}.

The surface morphologies of the raw and CNM-coated cotton, cotton/polyamide, and polyester samples with equal concentration and layers number are depicted in Fig. 15. The surface of the CNM-covered cotton/polyamide and polyester samples are relatively smoother and freer of roughness compared to the cotton. Due to the lower density of the cotton's texture and the voids between its warp and weft, a lower amount of conductive paste was introduced on the surface of the fabrics.

As can be observed in Fig. 15 (b) the cotton fibres are exposed on the surface of the CNM-covered sample. Indeed, a significant amount of the paste is used to fill the pores between the threads or wasted through the spaces between the fabric warp and weft. Hence, more print layers are required to fully cover the fabric surface and creation of a continuous conductive layer. Although the thickness of the printed conductive layer on cotton samples is less than cotton/polyamide and polyester, its total thickness is relatively equal due to the twist and the voids between the fibres forming the warp and also the weft of the cotton. Hence the electrical resistivity of the cotton samples is roughly higher than cotton/polyamide and polyester coated with the same number of layers.

The possible discontinuity in the conductive layer caused by shrinkage of the CNM paste during the curing process can affect the electrical conductivity of the cotton sample due to the higher water absorption of the cotton fibres [123] and the lower thickness of the conductive layer. However, these aspects require more detailed investigations.

As shown in Fig. 15, the surface of the CNM-coated samples includes spherical porosities. The presence of these porosities in the conductive layer might be due to the presence of foam (air entrapment inside the viscose paste during the high-speed mixing process) or evaporation of water and/or acetone remaining in the conductive paste. Although these porosities may reduce the conductivity of the sample, they can increase its sensitivity to stress changes due to the elasticity of the paste. These porosities on the surface also can enhance the interface condition, interaction and adhesion of the TPU waterproof layer with the conductive paste.

The surface and section morphologies of the CNMs-coated and TPU-covered cotton, cotton/polyamide, and polyester samples with equal concentration and layers number are illustrated in Fig. 16. The surface of the TPU-covered polyester sample is smoother than cotton and cotton/polyamide. As shown in Fig. 16, although the total thickness of the samples is equal, the thickness of the conductive and TPU layer on the polyester fabrics is significantly more than cotton/polyamide and cotton samples. Meanwhile, there is a proper interaction and intertwining between the set of conductive paste and the waterproof layer and fabric texture in the polyester sample.

The XRD pattern of the raw and TPU-covered samples for different cotton, cotton/polyamide, and polyester fabrics are presented in Fig. 17. The diffraction patterns of covered samples are almost the same as that of pure fabrics. In raw cotton and cotton/polyamide, the diffraction peaks at 14.96°, 16.50°, 22.74°, and 34.14° are attributed to the (1–10), (110), (200), and (004) crystal faces of cellulose Iβ, respectively [124,125]. However, the peaks are less intense in the raw cotton/

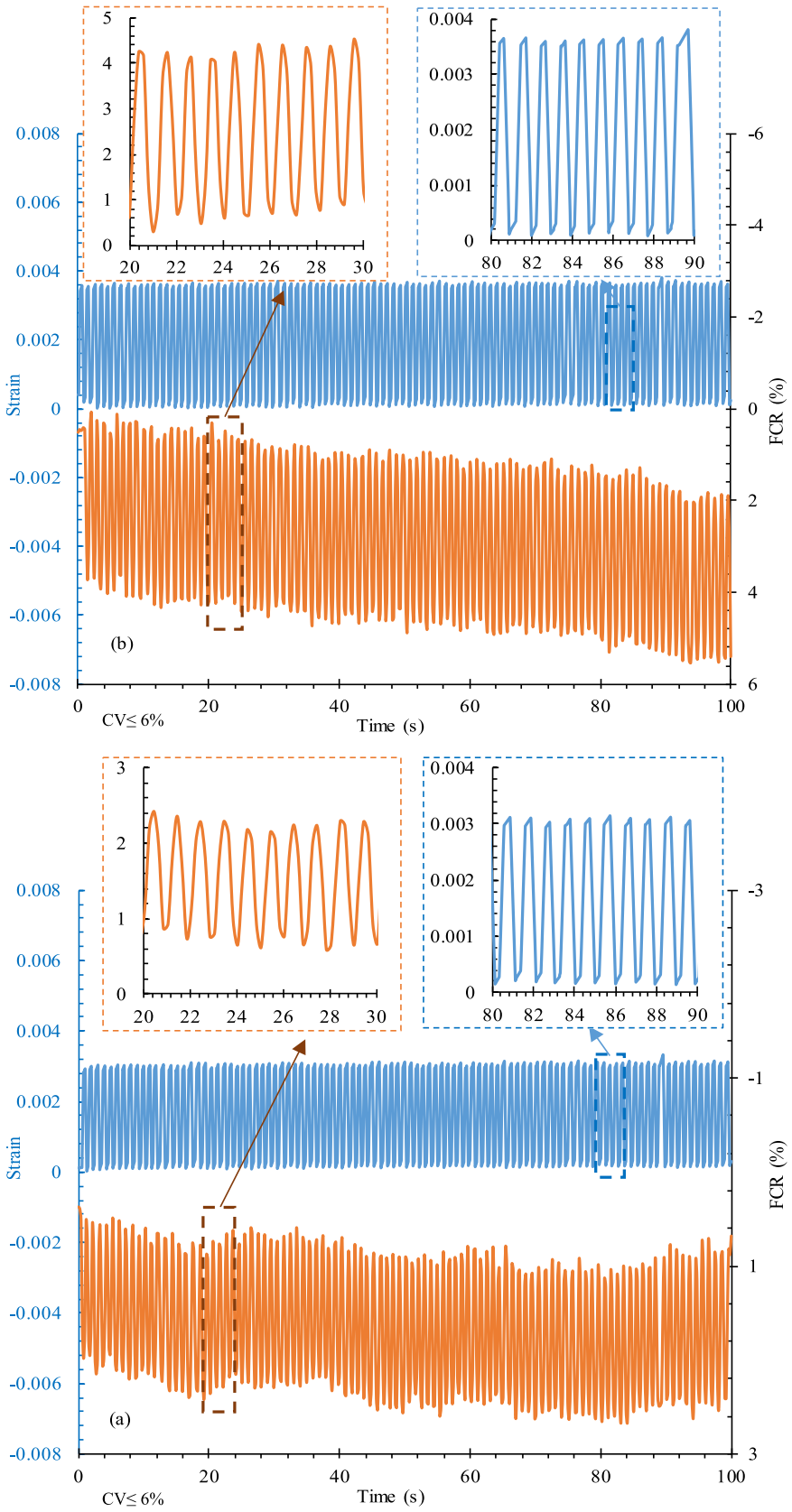


Fig. 23. Piezoresistive responses of the cementitious composites reinforced with different smart elements under fatigue flexural loading: a) C (5.0%)- 4L, b) C/PA (4.0%)- 4L, c) PL (4.0%)- 4L.

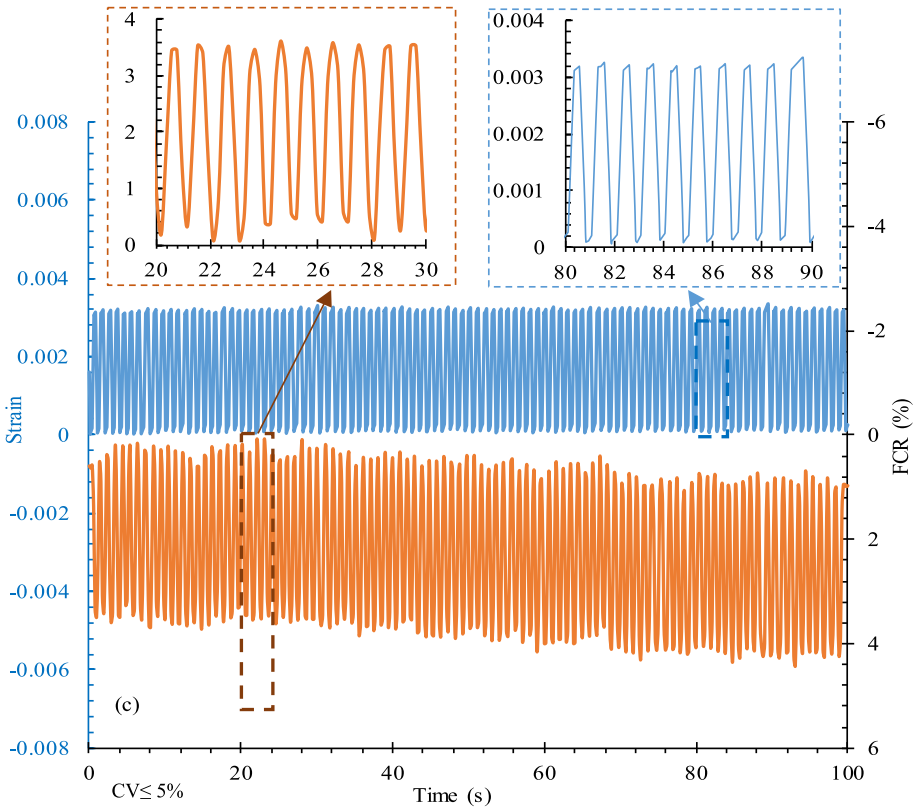


Fig. 23. (*continued*).

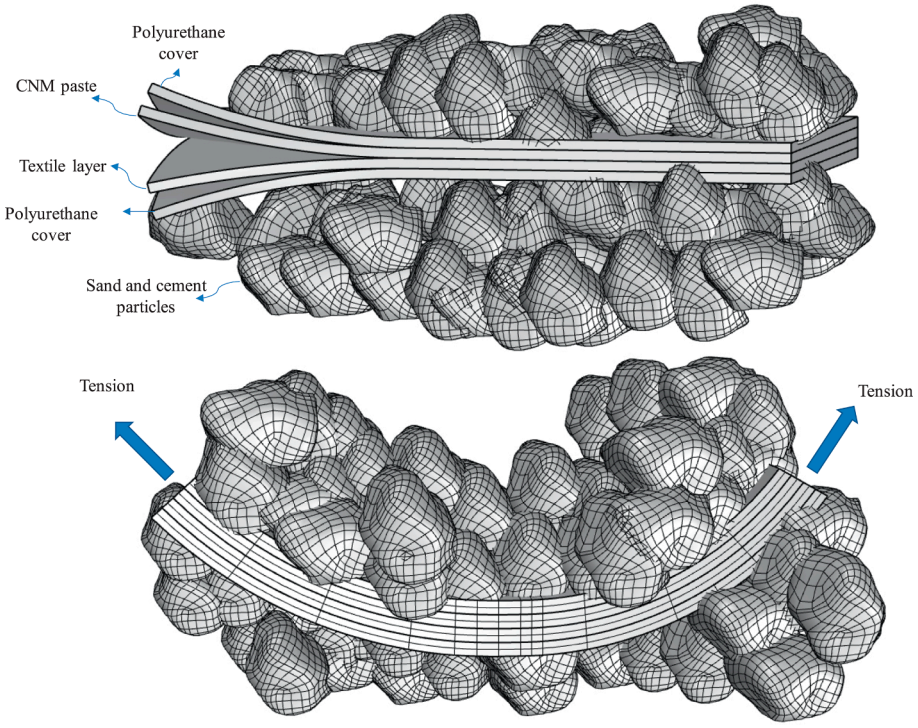


Fig. 24. Schematic representation of the SPC embedded in a cementitious composite.

polyamide sample. In raw polyester fabric, the reflection peaks at 17.4°, 22.7° and 25.4° correspond to (100), (002), and (101) planes of polyester [126,127]. The new diffraction peaks at around 8°, 19°, and 26.3° in all TPU-covered samples, might be indexed as crystallinity polyurethane chains with regular interplanar spacing and the C (002) reflection of graphite of CNTs and GNPs [128,129]. Moreover, in the covered samples, the intensities of diffraction peaks of raw fabrics slightly decreased.

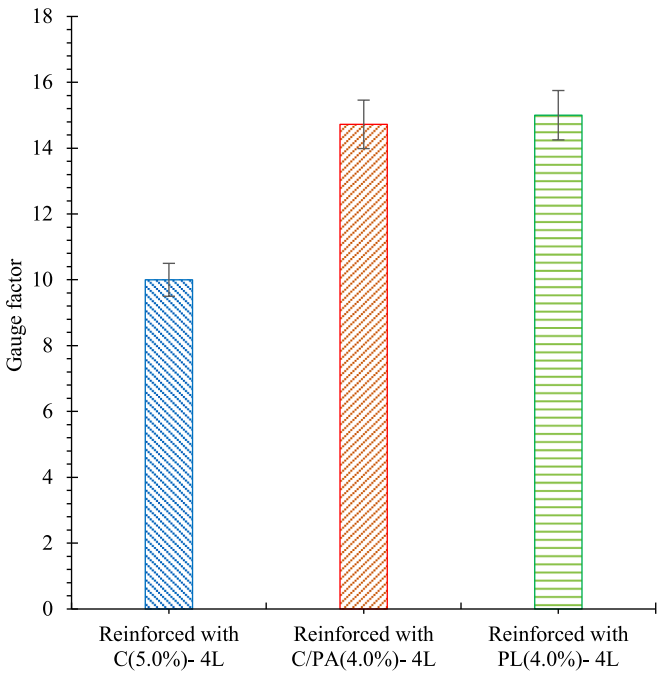


Fig. 25. Gauge factor values for different cementitious specimens reinforced with smart elements of cotton, cotton/polyamide, and polyester.

The results of thermography analysis for different TPU-covered cotton, cotton/polyamide, and polyester samples coated with equal CNM concentration and printing layer are shown in Fig. 18. Considering the rapid depolymerization of hemicellulose, lignin, and polyurethane matrices, the maximum decomposition temperature of all samples was in the range of 250 °C to 450 °C. Water evaporation caused a weight loss near 100 °C in all samples due to the hygroscopic nature of the fabric material. A Similar trend was reported in prior studies [98,130]. Thermal degradation graphs (Fig. 18 (a)) indicated maximum weight loss rate at 344-358℃ and 399-413℃, which related to the degradation of α-cellulose of the fabrics and set of conductive paste and TPU layer, respectively. As shown in Fig. 18 (b), the weight loss of the cotton sample affected by thermal decomposition, is lower than cotton/polyamide, and polyester. These results generally evident a higher amount of conductive paste in polyester samples.

3.4. Cementitious composite reinforced with smart textile

3.4.1. Pull-out test

A comparison of pull-out behaviour for different SPC samples is presented in Fig. 19. Three major regions were observed at pull-out load slip curves which are typical for successful tests. Initially, in the first zone, a stable strips debonding process occurs along the strip–cementitious matrix interface. In this region, there is no movement in the strip embedded length and the pull-out resistance by the strip increases up to the maximum load (P_{max}). At this stage, the displacements correspond to the elastic stretching of the debonded strip and the strip-free length. Then, in the second zone, the load decreases from P_{max} to frictional pull-out load (P_{fr}). The significant drop in this stage reveals the chemical bond breakage between the strip and the cementitious matrix and/or surface roughness. The sharp drops in the cotton sample might be due to the roughness of its surface which was discussed earlier. At point P_{fr}, the strip is fully debonded. In the third zone, which is the slippage zone, the strip load is resisted by frictional forces [131–134]. As shown in Fig. 19, the results did not show significant changes in shear bond strength for all SPC samples. The average shear bond strength of the cotton/polyamide sample was 8 and 20% higher than the cotton and polyester samples, respectively.

3.4.2. Mechanical assessment

The main mechanical characteristics of the cementitious composite reinforced with different SPC including cotton, cotton/polyamide, and polyester, are presented in Fig. 20. As can be observed, reinforcing cementitious composite with SPC elements in the tensile zone under flexural loading does not have significant effects on the mechanical behaviour of the specimen in the pre-crack zone due to the lower elastic modulus of the SPCs compared to the cementitious mortar. However, by comparing plain specimens with those reinforced, it is obvious that the SPC elements increased the failure strain of the specimen in the post-crack region and prevented its sudden failure.

As shown in Fig. 20, there was a significant increase in toughness (area under the stress–strain curve) with reinforcing cementitious composites by SPC elements. The toughness of cementitious composites represents the ability to absorb energy and resist plastic deformation during fracture. As a result of better toughness, fewer cracks and fractures occur, which is beneficial to increase the materials' durability [135]. As shown in Fig. 20, the plain specimen had a brittle fracture, where the loading force decreases suddenly after reach to maximum strength. As compared to plain samples, specimens reinforced with SPCs exhibit higher ductility and distinct post-peak toughness. Loading forces of the reinforced specimens increased linearly with strain increments, but sharply decreased when cracks appeared leading to the load transfer from the cement matrix to the SPCs and resulting in another increase. In particular, the change in the stress–strain curve of the specimen reinforced with polyester SPC is more obvious. When the strain increases, the specimen's loading force exhibits steady growth due to the tensile resistance of SPCs, until the maximum bond strength or tensile strength of the specimen is reached. Then, there exists a descending stage since the energy is released by the generation of cracks, extruding of SPC (in

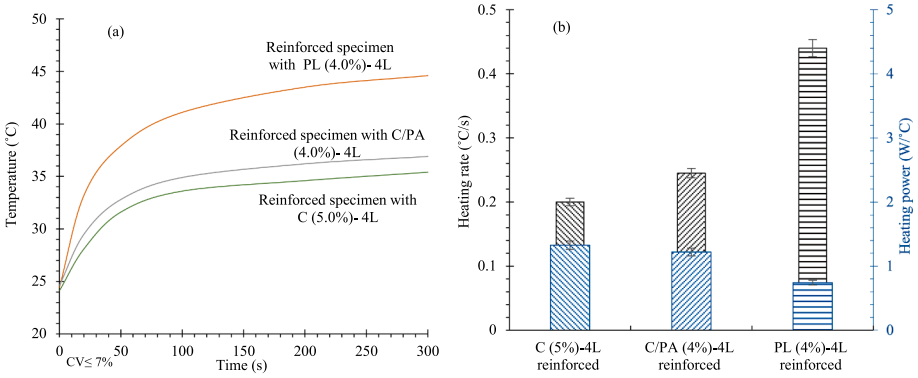


Fig. 26. Self-heating (joule heating) performance of the cementitious specimen reinforced with different smart elements: a) heating trend, b) heating rate and heating power.

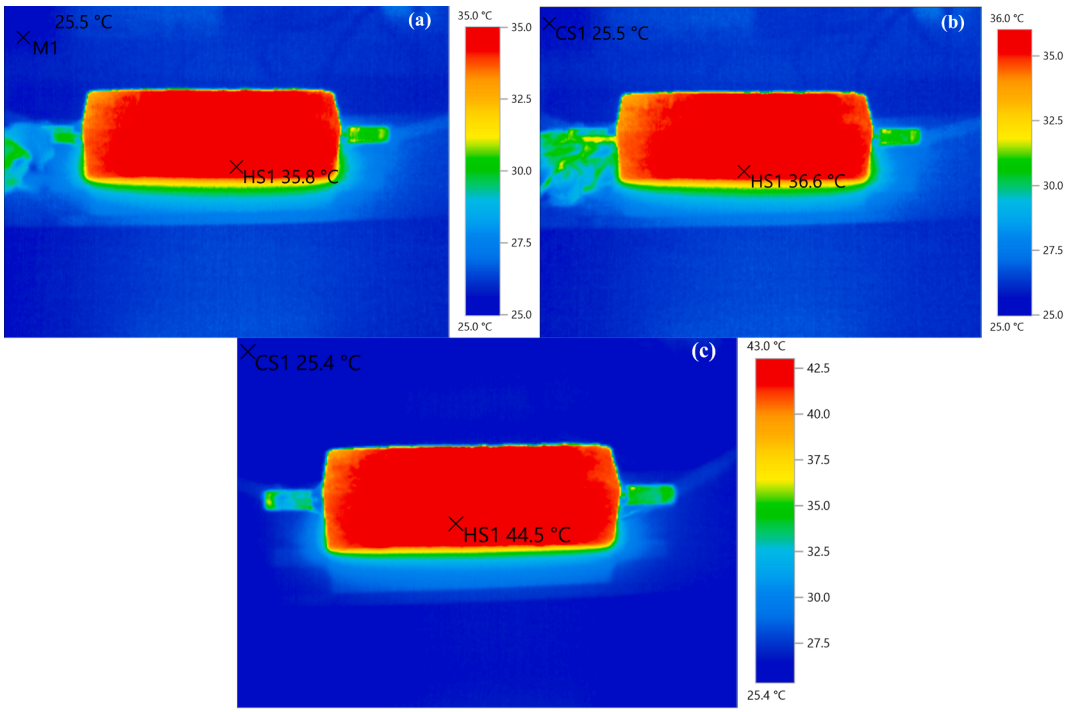


Fig. 27. Thermographic images of the cementitious specimen reinforced with different smart elements: a) C (5.0%)- 4L, b) C/PA (4.0%)- 4L, c) PL (4.0%)- 4L.

Table 6
Comparison of heating performance in cementitious composites with different methods.

Heating technique	Maximum increase in temperature (℃)	Voltage (V)	Heating rate (℃/min)	Remarks	References
Self-heating concrete	59	25 DC	1.93	1.5 vol% of steel fibers	[8]
Self-heating concrete	77	20 DC	–	0.4 vol% carbon fiber + 0.8 vol% carbon black	[27]
Incorporating phase change materials in concrete	20	–	0.07	Embedded pipes to 14.0 vol%. 22.1 vol% of Paraffin oil as phase change materials	[37]
Concrete coating with conductive polymer	50	20 AC	16	Polyurethane + Carbon fibers (20 vol%)	[31]
Self-heating braided planar composite	44.5	25 DC	15.2	polyester coated with 4 layers of hybrid water-based polymeric resins containing 4% CNT/GNP	Present study

the case of bond slipping), and tearing of SPCs fibers.

The nature of the multiple cracking, toughness, and strength of the cement composite are all influenced by the properties of the SPCs and matrix, and SPCs-matrix interface bonding [52]. Hence, the specimens containing cotton/polyamide, cotton and polyester SPCs exhibited more toughness respectively. However, the specimen reinforced with polyester SPCs showed higher maximum strength. In general, a high-strength and modulus fiber will usually increase the strength and toughness of the cement composite, providing a strain-hardening behaviour. While in low-modulus fiber, the reinforcement enhances mainly the ductility of the cement composite, but not its strength, resulting in strain-softening or elastic–plastic behaviour [52].

As shown in Fig. 20 (b), reinforcing the cementitious specimen with cotton, cotton/polyamide, and polyester SPC increased the flexural strength by approximately 18, 19, and 50% respectively. The failure strain of the specimens was also improved by around 1.23, 1.8, and 1.18 times respectively.

3.4.3. *Self-sensing performance*

The piezoresistive behaviour of the cementitious specimens reinforced with different SPC including cotton, cotton/polyamide, and polyester under different flexural loading are illustrated in Fig. 21, Fig. 22, and Fig. 23.

As can be observed there is proper conformity and correlation between the amounts of FCR and strain changes in all types of loading patterns. Increasing the stress, caused an increase in strain and consequently increased the FCR. As shown in Fig. 21, the maximum changes in electrical resistivity of the reinforced specimen with cotton, cotton/polyamide, and polyester under similar creep flexural cyclic loading (1000 N ≈ 2.3 MPa) were approximately 2.6, 5.1, and 4.2% respectively. The results showed a similar trend for the strain changes.

As shown in Fig. 22, in incremental multiple flexural loading, a proper correlation between FCR and strain was also obtained. Increasing the cyclic load to 500 (≈1.17 MPa), 1000 (≈2.3 MPa), and 1500 N (≈ 3.5 MPa), caused an increase in electrical resistivity of the cotton-reinforced specimens by around 1.8, 2.7, and 3.8% respectively. These amounts for cotton/polyamide and polyester-reinforced cementitious composites were approximately 3.3, 5.3, and 7.1 %and 2.4, 4.4, and 6.6% respectively. As mentioned before, self-sensing or self-diagnosing composites arise from the dispersion of a conductive phase in a non-conductive matrix. These conductive phases create an extensive network of conductive pathways based on quantum tunnelling effects and percolation theory which are disturbed or changed if the composite is stressed or deformed under external force [6]. Following the percolation mechanism, when the concentration of conductive phases exceeds a certain threshold, the conductive filler particles are in physical contact together, which forms an extensive conductive network within the associated matrix [5,91,136].

The piezoresistive behaviour of the SPC-reinforced cementitious composite under long-term flexural cyclic loading (Fig. 23), showed a proper correlation between strain and electrical resistivity changes. However, a relatively low instability appeared in the FCR values due to polarization effects. Electric polarization is known as the separation of the centre of negative and positive charges in a material. A sufficiently high electric field can cause this separation [137]. The polarization induces an increase in the measured electrical resistivity of the SPC during resistivity measurement. This increase for cotton, cotton/polyamide, and polyester-reinforced specimens was approximately 1.2, 0.6, and 0.4%. The polarization effect can be diminished by increasing the conductivity of the SPCs and using alternating currents (AC) [138].

The changes in resistance as a result of the applied load can be explained via two main mechanisms (Fig. 24), disturbances and pressure on the conductive paths formed in the conductive paste, caused by sand and cement grains, damage and tensile strains of the conductive paste due to the bending strain of the cementitious specimen. However, in the quantum tunnelling mechanism, the electrical conductivity of the composite is enabled by the transfer of electrons between adjacent filler particles in the matrix under an external electric field [5]. Increasing the distance between conductive elements (CNMs) or disrupting the conductive paths increases the specimen's electrical resistance. The recoverability of the SPC after each loading cycle is one of the points of interest in these composites, which are created thanks to polyurethane-based polymeric resins and the nature of braided composites. However, in the case of using epoxy resins, the recoverability of the planar-braided composites is much lower due to low interlaminar toughness and the brittle nature of most epoxy matric [48,81].

The gauge factor values for different cementitious specimens reinforced with smart elements including cotton, cotton/polyamide, and polyester are presented in Fig. 25. As mentioned, the gauge factor is a criterion to express the sensitivity of the specimens to strain changes. The cementitious specimen reinforced with cotton/polyamide and polyester smart element offered a higher gauge factor. As shown, the number of changes in electrical resistivity of these samples was approximately 15 units for each unit change in the flexural strain. However, each unit change in the strain of cementitious composite reinforced with the cotton smart element under flexural loading caused 10 unit changes in the electrical resistivity.

Generally, these results showed a higher sensitivity of the reinforced specimen with cotton/polyamide and polyester smart elements against the strain and consequently stress changes.

3.4.4. Self-heating performance

The electrical heating capability of the cementitious composites reinforced with cotton, cotton/polyamide, and polyester smart elements are shown in Fig. 26 and Fig. 27. In these investigations, a 25 V DC was employed. The temperature of the specimens reinforced with cotton, cotton/polyamide, and polyester smart elements influenced by the ohmic heating effect, increased to 35, 36, and 44 ℃. During the 300 s joule heating tests process, all the specimens showed a similar trend with different heating rates.

The heating rate of the cementitious specimens reinforced with cotton, cotton/polyamide, and polyester smart elements in the initial steps of the ohmic heating process were approximately 0.2, 0.25, and 0.44 ℃/s respectively. The joule heating power of these specimens was also 1.3, 1.2, and 0.7 W/C respectively. A Comparison of the heating performance of different methods in cementitious composites in prior studies is presented in Table 6.

4. Conclusions

In this study, smart planar braided composites (SPCs) with reinforcing, self-sensing and self-heating capabilities were developed using printing a conductive paste composed of hybrid water-based polymeric resins, carbon nanotubes (CNTs)/graphene nanoplatelets (GNPs) on cotton, cotton/polyamide, and polyester fabrics. The samples were covered by a waterproof thermoplastic polyurethane (TPU) resin using knife coating after the curing process. Mechanical, microstructural, joule heating and self-sensing performance of samples were assessed using various tests and the following results were drawn:

- Electrical conductivity measurement of the SPCs indicated a reduction in percolation threshold concentration with an increasing number of printing layers. Generally, the electrical conductivity of the polyester samples was more than cotton/polyamide and cotton samples coated with equal CNMs percentage and printing layers' number due to the higher density and lower surface pores which showed the significant impacts of the physical properties of the fabric in this method.
- The comparison of pull-out behaviour for different SPC samples showed a higher shear bond strength of the cotton/polyamide sample by approximately 8 and 20% compared to cotton and polyester respectively. The results also indicated a higher frictional pull-out load of cotton samples due to the roughness of their surface.
- Reinforcing the cementitious specimen with cotton, cotton/polyamide, and polyester SPC increased the flexural strength by approximately 18, 19, and 50% respectively. The failure strain of the specimens was also improved by around 1.23, 1.8, and 1.18 times respectively. Generally, the SPC elements improved the post-crack behaviour of the cementitious specimen and prevents its sudden failure.
- The piezoresistive behaviour of the cementitious composite reinforced with smart elements of cotton, cotton/polyamide, and polyester under flexural cyclic loading showed changes in their electrical resistivity by approximately 2.6, 5.1, and 4.2% respectively. The high sensitivity and correlation between electrical resistance and strain and consequently stress under different flexural cyclic loading protocols proved the high potential of the composite for various applications including structural health monitoring, transportation, and traffic detection.
- The temperature of the cementitious specimens reinforced with cotton, cotton/polyamide, and polyester smart elements influenced by the joule heating effect (25 V/DC), increased to 35, 36, and 44 ℃ respectively. A heating rate of 0.44 ℃/s and a joule heating power of 0.7 W/C indicated the high heating capabilities of these composites to be used in various fields such as de-icing and self-healing.

In summary, the results showed that polyester coated with 4 layers of hybrid water-based polymeric resins containing 4% CNT/GNP is a proper candidate for multifunctional planar composite development for reinforcing, self-sensing and self-heating functions.

5. Future research lines

The above outcomes proved the potentiality of the developed technique for generating multifunctional braided planar composite with reinforcing, self-sensing, and self-heating capabilities for different civil infrastructures. The main advantages of the SPCs include low cost and simple production process, easy transportation and installation, and simple and common equipment for operation during the service life. It should be noted that apprehension about the high cost of carbon nanomaterials had always made their mass use challenging, while thanks to the ever-increasing advancements in this technology as well as using of waste materials for industrial grade CNMs production, its cost has significantly decreased [139–141]. Moreover the low thickness of the conductive paste (<200 μm) and composed of 4% CNT/GNP reduced the price of each square meter of this composite to less than one ∈.

However, due to the novelty of the concept and the lack of knowledge about the development of this multifunctional composite for civil application, three common fabrics were used to bridge the existing knowledge and ensure concept efficiency.

Indeed this study is a starting point and draws a perspective for future assessments. Considering various applications of this multifunctional composite in civil projects including transportation infrastructure, structural elements, and smart geosynthetics development, the further relative investigation is suggested. It is vital to evaluate the associated environmental impacts of SPCs through the Life Cycle Assessment as one of the important aspects of all multifunction composites [142–144].

The designing factors including various host braided matrices with different mechanical behaviour and durability, the thickness of the waterproof layer, and the density and shape of printed electrical circuits for adjusting the resolution and localization of the detected parameters or heated efficiency, need to be optimized based on the intended application. Moreover, with the optimization of the design items based on the application, the proper production method for mass production can be achieved which reduces the costs and environmental impacts of this multifunctional composite.

6. Data availability statement

Requests for all types of data used to support the findings of this study, after the publication of this article, will be considered by the corresponding author, subject to obtaining permission from the owners.

CRediT authorship contribution statement

Mohammadmahdi Abedi: Conceptualization, Methodology, Formal analysis, Validation, Investigation, Resources, Data curation, Writing – original draft, Writing – review & editing, Visualization, Supervision, Project administration. **Usha Kiran Sanivada:** Methodology, Formal analysis, Validation, Investigation, Resources, Data curation, Writing – original draft, Writing – review & editing, Visualization. **Seyed Ali Mirian:** Formal analysis, Validation, Investigation, Resources, Data curation, Writing – original draft, Visualization. **Omid Hassanshahi:** Investigation. **Khalifa Al-Jabri:** Methodology, Formal analysis, Validation, Investigation, Resources. **António Gomes Correia:** Supervision, Resources, Writing – review & editing. **Paulo B. Lourenço:** Methodology, Validation, Writing – review & editing, Supervision, Resources. **Raul Fangueiro:** Conceptualization, Methodology, Formal analysis, Validation, Resources, Writing – review & editing, Supervision, Funding acquisition.

Declaration of Competing Interest

The authors declare that they have no known competing financial interests or personal relationships that could have appeared to influence the work reported in this paper.

Data availability

Data will be made available on request.

Acknowledgements

This work was partly financed by the Institute for Sustainability and Innovation in Engineering Structures (ISISE) and the R&D Unit of the Centre for Textile Science and Technology (2C2T) founded by the Portuguese Foundation for Science and technology (FCT) under the reference “UIDP/00264/2020”. The first author also acknowledges the support provided by the FCT/PhD individual fellowship with reference of “2021.07596.BD”.

References

[1] Y. Kaluarachchi, Potential advantages in combining smart and green infrastructure over silo approaches for future cities, Front. Eng. Manag. 8 (2021) 98–108, https://doi.org/10.1007/s42524-020-0136-y.
[2] S.E. Bibri, Data-driven smart sustainable cities of the future: An evidence synthesis approach to a comprehensive state-of-the-art literature review, Sustain. Futur. 3 (2021) 100047, https://doi.org/10.1016/j.sftr.2021.100047.
[3] P. Zare, S.S. Narani, M. Abbaspour, A. Fahimifar, S.M.M.M. Hosseini, P. Zare, Experimental investigation of non-stabilized and cement-stabilized rammed earth reinforcement by Waste Tire Textile Fibers (WTTFs), Constr. Build. Mater. 260 (2020) 120432.
[4] S.S. Narani, P. Zare, M. Abbaspour, A. Fahimifar, S. Siddiqua, S.M.M.M. Hosseini, Evaluation of fiber-reinforced and cement-stabilized rammed-earth composite under cyclic loading, Constr. Build. Mater. 296 (2021) 123746.
[5] W. Dong, W. Li, Z. Tao, K. Wang, Piezoresistive properties of cement-based sensors: Review and perspective, Constr. Build. Mater. 203 (2019) 146–163, https://doi.org/10.1016/j.conbuildmat.2019.01.081.
[6] M. Abedi, R. Fangueiro, A. Gomes Correia, A review of intrinsic self-sensing cementitious composites and prospects for their application in transport infrastructures, Constr. Build. Mater. 310 (2021) 125139, https://doi.org/10.1016/j.conbuildmat.2021.125139.
[7] M. Abedi, R. Fangueiro, A. Gomes Correia, Ultra-sensitive affordable cementitious composite with high mechanical and microstructural performances by hybrid CNT/GNP, Materials (Basel) 13 (2020) 3484.
[8] S. Ding, S. Dong, X. Wang, S. Ding, B. Han, J. Ou, Self-heating ultra-high performance concrete with stainless steel wires for active deicing and snow-melting of transportation infrastructures, Cem. Concr. Compos. 138 (2023) 105005, https://doi.org/10.1016/j.cemconcomp.2023.105005.
[9] D.D.L. Chung, Self-heating structural materials, Smart Mater. Struct. 13 (3) (2004) 562–565.
[10] H. Lee, W. Yu, K.J. Loh, W. Chung, Self-heating and electrical performance of carbon nanotube-enhanced cement composites, Constr. Build. Mater. 250 (2020) 118838.
[11] H. Bao-guo, O.u. Jin-ping, Humidity sensing property of cements with added carbon, New Carbon Mater. 23 (4) (2008) 382–384.
[12] A. Di Graziano, V. Marchetta, S. Cafiso, Structural health monitoring of asphalt pavements using smart sensor networks: a comprehensive review, J. Traffic Transp. Eng. (English Ed. 7 (5) (2020) 639–651.
[13] M. Abedi, R. Fangueiro, A.G. Correia, Effects of multiscale carbon-based conductive fillers on the performances of a self-sensing cementitious geocomposite, J. Build. Eng. 43 (2021) 103171.
[14] J. Pelton, I. Singh, Smart cities of today and tomorrow, Cham Springer Int. Publ. (2019).
[15] M. Abedi, O. Hassanshahi, J.A.O. Barros, A. Gomes Correia, R. Fangueiro, Three-dimensional braided composites as innovative smart structural reinforcements, Compos. Struct. 297 (2022) 115912.
[16] M. Won, Intelligent traffic monitoring systems for vehicle classification: a survey, IEEE Access. 8 (2020) 73340–73358.
[17] Z. Ye, H. Xiong, L. Wang, Collecting comprehensive traffic information using pavement vibration monitoring data, Comput. Civ. Infrastruct. Eng. 35 (2) (2020) 134–149.
[18] F.-G. Yuan, S.A. Zargar, Q. Chen, S. Wang, Machine learning for structural health monitoring: challenges and opportunities, Sensors Smart Struct. Technol. Civil, Mech. Aerosp. Syst. 2020 (11379) (2020) 1137903.
[19] S. Hassani, U. Dackermann, A systematic review of advanced sensor technologies for non-destructive testing and structural health monitoring, Sensors 23 (2023) 2204.
[20] T. Singh, S. Sehgal, Structural health monitoring of composite materials, Arch. Comput. Methods Eng. 1–21 (2021).
[21] M.S. Irfan, M.A. Ali, K.A. Khan, R. Umer, A. Kanellopoulos, Y. Abdul Samad, An electronic textile embedded smart cementitious composite, Eng. Rep. 4 (2022) 1–12, https://doi.org/10.1002/eng2.12468.
[22] K.-H. Tseng, C.K. Soh, A. Gupta, S. Bhalla, Health monitoring of civil infrastructure using smart piezoelectric transducer patches, WIT Trans. Built Environ. 46 (2000).
[23] M. Abedi, R. Fangueiro, A. Gomes Correia, Innovative self-sensing fiber-reinforced cemented sand with hybrid CNT/GNP, Smart Mater. Struct. 30 (10) (2021) 105034.
[24] B. Han, X. Guan, J. Ou, Electrode design, measuring method and data acquisition system of carbon fiber cement paste piezoresistive sensors, Sensors Actuators A Phys. 135 (2) (2007) 360–369.
[25] J. Zhang, R. She, S. Xia, Z. Dai, N. Hu, X. Cui, R. Han, R. Ming, G. Ma, Development and laboratory evaluation of a self-monitoring polymer geobelts, Measurement 166 (2020) 108214, https://doi.org/10.1016/j.measurement.2020.108214.
[26] J. Li, X. Cui, Q. Jin, J. Su, S. Cui, Y. Wang, Laboratory investigation of the durability of a new smart geosynthetic material, Constr. Build. Mater. 169 (2018) 28–33, https://doi.org/10.1016/j.conbuildmat.2018.02.187.
[27] S. Gwon, H. Kim, M. Shin, Self-heating characteristics of electrically conductive cement composites with carbon black and carbon fiber, Cem. Concr. Compos. 137 (2023) 104942.
[28] S. Gwon, J. Moon, M. Shin, Self-heating capacity of electrically conductive cement composites: Effects of curing conditions, Constr. Build. Mater. 353 (2022) 129087.
[29] R. Jian, X. Hu, T. Han, J. Wan, W. Gan, Z. Chen, Y. Zhang, C. Cao, Optimization of induction heating parameters for improving self-healing performance of asphalt mixture through partial least square model, Constr. Build. Mater. 365 (2023) 130019.

[30] S.M.S. Sadati, K.S. Cetin, H. Ceylan, S. Kim, Energy-efficient design of a carbon fiber-based self-heating concrete pavement system through finite element analysis, Clean Technol. Environ. Policy 22 (5) (2020) 1145–1155.

[31] A. Sassani, A. Arabzadeh, H. Ceylan, S. Kim, K. Gopalakrishnan, P.C. Taylor, A. Nahvi, Polyurethane-carbon microfiber composite coating for electrical heating of concrete pavement surfaces, Heliyon 5 (8) (2019) e02359.

[32] S.M.S. Sadati, K. Cetin, H. Ceylan, A. Sassani, S. Kim, Energy and thermal performance evaluation of an automated snow and ice removal system at airports using numerical modeling and field measurements, Sustain. Cities Soc. 43 (2018) 238–250.

[33] K. Liu, S. Huang, F. Wang, H. Xie, X. Lu, Energy consumption and utilization rate analysis of automatically snow-melting system in infrastructures by thermal simulation and melting experiments, Cold Reg. Sci. Technol. 138 (2017) 73–83.

[34] K. Liu, C. Fu, H. Xie, F. Wang, X. Wang, H. Bai, Design of electric heat pipe embedding schemes for snow-melting pavement based on mechanical properties in cold regions, Cold Reg. Sci. Technol. 165 (2019) 102806.

[35] J.W. Daniels, E. Heymsfield, Development of anti-icing airfield pavement using surface-embedded heat wire, Int. J. Pavement Eng. 21 (6) (2020) 725–735.

[36] M.A. Montoya, R. Rahbar-Rastegar, J.E. Haddock, Incorporating phase change materials in asphalt pavements to melt snow and ice, Int. J. Pavement Eng. 1–14 (2022).

[37] Y. Farnam, H.S. Esmaeeli, P.D. Zavattieri, J. Haddock, J. Weiss, Incorporating phase change materials in concrete pavement to melt snow and ice, Cem. Concr. Compos. 84 (2017) 134–145.

[38] C. Chen, Z.e. Tian, X. Luo, G. Jiang, X. Hu, L. Wang, R. Peng, H. Zhang, M. Zhong, Micro–nano-nanowire triple structure-held PDMS superhydrophobic surfaces for robust ultra-long-term icephobic performance, ACS Appl. Mater. Interfaces 14 (20) (2022) 23973–23982.

[39] Z. Hou, Z. Li, J. Wang, Electrically conductive concrete for heating using steel bars as electrodes, J. Wuhan Univ. Technol. Sci. Ed. 25 (3) (2010) 523–526.

[40] C. Gürer, U. Fidan, B.E. Korkmaz, Investigation of using conductive asphalt concrete with carbon fiber additives in intelligent anti-icing systems, Int. J. Pavement Eng. 24 (1) (2023).

[41] M.A. Notani, A. Arabzadeh, H. Ceylan, S. Kim, K. Gopalakrishnan, Effect of carbon-fiber properties on volumetrics and ohmic heating of electrically conductive asphalt concrete, J. Mater. Civ. Eng. 31 (2019) 4019200.

[42] X. Zhu, Q. Zhang, Z. Du, H. Wu, Y. Sun, Snow-melting pavement design strategy with electric cable heating system balancing snow melting, energy conservation, and mechanical performance, Resour. Conserv. Recycl. 177 (2022) 105970.

[43] W. Jiao, A. Sha, Z. Liu, W. Li, L. Zhang, S. Jiang, Optimization design and prediction of the snow-melting pavement based on electrical-thermal system, Cold Reg. Sci. Technol. 193 (2022) 103406.

[44] H. Yazdani, K. Hatami, Sensor-enabled geogrids for stabilization and performance monitoring of earth structures: state of development, Int. J. Geosynth. Gr. Eng. 2 (2016) 37, https://doi.org/10.1007/s40891-016-0077-z.

[45] H. Yazdani, B.E. Smith, K. Hatami, Electrical conductivity and mechanical performance of multiwalled CNT-filled polyvinyl chloride composites subjected to tensile load, J. Appl. Polym. Sci. 133 (29) (2016).

[46] M. Abedi, R. Fangueiro, A. Camões, A. Gomes Correia, Evaluation of CNT/GNP's synergic effects on the mechanical, microstructural, and durability properties of a cementitious composite by the novel dispersion method, Constr. Build. Mater. 260 (2020) 120486, https://doi.org/10.1016/j.conbuildmat.2020.120486.

[47] M.A. Arjomand, M. Abedi, M. Gharib, M. Damghani, An experimental study on geogrid with geotextile effects aimed to improve clayey soil, Int. J. Eng. 32 (2019) 685–692.

[48] H. Zhang, Y. Liu, M. Kuwata, E. Bilotti, T. Peijs, Improved fracture toughness and integrated damage sensing capability by spray coated CNTs on carbon fibre prepreg, Compos. Part A Appl. Sci. Manuf. 70 (2015) 102–110, https://doi.org/10.1016/j.compositesa.2014.11.029.

[49] S. Rana, E. Zdraveva, C. Pereira, R. Fangueiro, A.G. Correia, Development of hybrid braided composite rods for reinforcement and health monitoring of structures, Sci. World J. 2014 (2014) 1–9.

[50] N. Fouad, M.A. Saifeldeen, Smart self-sensing fiber-reinforced polymer sheet with woven carbon fiber line sensor for structural health monitoring, Adv. Struct. Eng. 24 (1) (2021) 17–24.

[51] H. Ventura, M.D. Álvarez, L. Gonzalez-Lopez, J. Claramunt, M. Ardanuy, Cement composite plates reinforced with nonwoven fabrics from technical textile waste fibres: Mechanical and environmental assessment, J. Clean. Prod. 372 (2022) 133652, https://doi.org/10.1016/j.jclepro.2022.133652.

[52] A. Peled, A. Bentur, Fabric structure and its reinforcing efficiency in textile reinforced cement composites, Compos. Part A Appl. Sci. Manuf. 34 (2) (2003) 107–118.

[53] S.K. Shukla, Geosynthetics and ground engineering: sustainability considerations, Int. J. Geosynth. Gr. Eng. 7 (2021) 1–3.

[54] S. Nauman, Piezoresistive Sensing Approaches for Structural Health Monitoring of Polymer Composites—A Review, Eng 2021, Vol. 2, Pages 197-226. 2 (2021) 197–226. https://doi.org/10.3390/ENG2020013.

[55] M.H. Islam, S. Afroj, M.A. Uddin, D.V. Andreeva, K.S. Novoselov, N. Karim, Graphene and CNT-based smart fiber-reinforced composites: a review, Adv. Funct. Mater. 32 (40) (2022) 2205723.

[56] S.A. Mirdehghan, Fibrous polymeric composites, in: Eng. Polym. Fibrous Mater., Elsevier, 2021: pp. 1–58.

[57] M.M.M. Sahib, S.R. Salim, Influence of fiber hybridization on strength and toughness of RC beams, Civ. Eng. J. 8 (2022) 549–566.

[58] A.V. Nistratov, N.N. Klimenko, I.V. Pustynnikov, L.K. Vu, Thermal regeneration and reuse of carbon and glass fibers from waste composites, Emerg. Sci. J. 6 (2022) 967–984.

[59] M. Yagoub, M. Mellas, A. Benchabane, A. Zatar, Experimental characterization of a functionally graded composite using recycled steel fiber, Civ. Eng. J. 8 (2022) 879–894.

[60] D.H. Murcia, B. Çomak, E. Soliman, M.M. Reda Taha, Flexural behavior of a novel textile-reinforced polymer concrete, Polymers (Basel) 14 (1) (2022) 176.

[61] H. Montazerian, A. Dalili, A.S. Milani, M. Hoorfar, Piezoresistive sensing in chopped carbon fiber embedded PDMS yarns, Compos. Part B Eng. 164 (2019) 648–658, https://doi.org/10.1016/j.compositesb.2019.01.090.

[62] K.S.C. Kuang, C.Y. Tan, S.H. Chew, S.T. Quek, Monitoring of large strains in submerged geotextile tubes using plastic optical fibre sensors, Sensors Actuators A Phys. 167 (2) (2011) 338–346.

[63] R.K. Rowe, C.T. Gnanendran, Geotextile strain in a full scale reinforced test embankment, Geotext. Geomembr. 13 (1994) 781–806, https://doi.org/10.1016/0266-1144(94)00015-6.

[64] R.K. Rowe, B.LJ. Mylleville, A geogrid reinforced embarkment on peat over organic silt: a case history, Can. Geotech. J. 33 (1) (1996) 106–122.

[65] C.T. Gnanendran, A.P.S. Selvadurai, Strain measurement and interpretation of stabilising force in geogrid reinforcement, Geotext. Geomembr. 19 (2001) 177–194, https://doi.org/10.1016/S0266-1144(01)00004-8.

[66] Z.-F. Wang, J. Wang, Q.-M. Sui, X.-M. Liang, L. Jia, S.-C. Li, S.-d. Lu, Development and application of smart geogrid embedded with fiber Bragg grating sensors, J. Sensors 2015 (2015) 1–10.

[67] P. Lenke, S. Liehr, K. Krebber, F. Weigand, E. Thiele, Distributed strain measurement with polymer optical fiber integrated in technical textiles using the optical time domain reflectometry technique, in: Proc. 16th Int. Conf. Plast. Opt. Fibers, International Cooperative of Plastic Optical Fibers (ICPOF), 2007: pp. 21–24.

[68] I.R. Husdi, K. Nakamura, S. Ueha, Sensing characteristics of plastic optical fibres measured by optical time-domain reflectometry, Meas. Sci. Technol. 15 (2004) 1553.

[69] C.-Y. Hong, Y.-F. Zhang, G.-W. Li, M.-X. Zhang, Z.-X. Liu, Recent progress of using Brillouin distributed fiber optic sensors for geotechnical health monitoring, Sensors Actuators A Phys. 258 (2017) 131–145, https://doi.org/10.1016/j.sna.2017.03.017.

[70] Y. Goldfeld, S. Ben-Aarosh, O. Rabinovitch, T. Quadflieg, T. Gries, Integrated self-monitoring of carbon based textile reinforced concrete beams under repeated loading in the un-cracked region, Carbon N. Y. 98 (2016) 238–249, https://doi.org/10.1016/j.carbon.2015.10.056.

[71] M.S. Irfan, M.A. Ali, K.A. Khan, R. Umer, A. Kanellopoulos, Y. Abdul Samad, An electronic textile embedded smart cementitious composite, Eng. Rep. 4 (2022) e12468.

[72] M. Abedi, A. Gomes Correia, R. Fangueiro, Geotechnical and piezoresistivity properties of sustainable cementitious stabilized sand reinforced with recycled fibres, Transp. Eng. 6 (2021) 100096, https://doi.org/10.1016/j.treng.2021.100096.

[73] Y. Hessam, H. Kianoosh, H. Takumi, G.B. P., Atomic-Scale Simulation of Sensor-Enabled Geosynthetics for Health-Monitoring of Reinforced Soil Slopes and Embankments, Geo-Congress 2013. (2022) 1522–1528. https://doi.org/doi:10.1061/9780784412787.152.

[74] K. Hatami, A. Hassanikhah, H. Yazdani, B.P. Grady, Tensoresistive PVC coating for sensor-enabled geogrids, J. Nanomech. Micromech. 4 (2014) A4013016.

[75] X. Cui, S. Cui, T. Lu, L. Zhang, Y. Wang, J. Li, Evaluation of the performance of sensor-enabled geobelts after cyclic loading, Constr. Build. Mater. 185 (2018) 414–422, https://doi.org/10.1016/j.conbuildmat.2018.07.046.

[76] P.A. Eutionnat-Diffo, A. Cayla, Y. Chen, J. Guan, V. Nierstrasz, C. Campagne, Development of flexible and conductive immiscible thermoplastic/elastomer monofilament for smart textiles applications using 3D printing, Polymers (Basel) 12 (2020) 2300.

[77] Z.-S. Huang, J.-W. Shiu, T.-F. Way, S.-P. Rwei, A thermo-responsive random copolymer of poly (NIPAm-co-FMA) for smart textile applications, Polymer (Guildf) 184 (2019) 121917.

[78] H. Yazdani, B.E. Smith, K. Hatami, Multi-walled carbon nanotube-filled polyvinyl chloride composites: Influence of processing method on dispersion quality, electrical conductivity and mechanical properties, Compos. Part A Appl. Sci. Manuf. 82 (2016) 65–77, https://doi.org/10.1016/j.compositesa.2015.12.005.

[79] A. Fathi, K. Hatami, B.P. Grady, Effect of carbon black structure on low-strain conductivity of polypropylene and low-density polyethylene composites, Polym. Eng. Sci. 52 (3) (2012) 549–556.

[80] T. Yan, Y. Wu, W. Yi, Z. Pan, Recent progress on fabrication of carbon nanotube-based flexible conductive networks for resistive-type strain sensors, Sensors Actuators A Phys. 327 (2021).

[81] M.A. Ali, R. Umer, K.A. Khan, Y.A. Samad, K. Liao, W. Cantwell, Graphene coated piezo-resistive fabrics for liquid composite molding process monitoring, Compos. Sci. Technol. 148 (2017) 106–114, https://doi.org/10.1016/j.compscitech.2017.05.022.

[82] M.O. Faruk, A. Ahmed, M.A. Jalil, M.T. Islam, B. Adak, M.M. Hossain, S. Mukhopadhyay, Functional textiles and composite based wearable thermal devices for Joule heating: progress and perspectives, Appl. Mater. Today. 23 (2021) 101025.

[83] A. Li, J. He, W. Wang, C.e. Cui, S. Jiang, S. Jiang, W. Qin, C. Cheng, R. Guo, Self-heating and hydrophobic nanofiber membrane based on Ti3C2T x MXene/Ag nanoparticles/thermoplastic polyurethane for electromagnetic interference

shielding and sensing performance, Ind. Eng. Chem. Res. 61 (41) (2022) 15249–15260.
[84] H. He, Y. Qin, J. Liu, Y. Wang, J. Wang, Y. Zhao, Z. Zhu, Q. Jiang, Y. Wan, X. Qu, A wearable self-powered fire warning e-textile enabled by aramid nanofibers/MXene/silver nanowires aerogel fiber for fire protection used in firefighting clothing, Chem. Eng. J. 460 (2023).
[85] M.K. Sarkar, J. Fan, Textiles for heat generation, in: Funct. Tech. Text., Elsevier, 2023: pp. 397–418.
[86] M. Abedi, R. Fangueiro, A.G. Correia, Development of a novel multifunctional cementitious-based geocomposite by the contribution of cnt and gnp, Nanomaterials 11 (2021) 1–28, https://doi.org/10.3390/nano11040961.
[87] M. Abedi, R. Fangueiro, A.G. Correia, An effective method for hybrid CNT/GNP dispersion and its effects on the mechanical, microstructural, thermal, and electrical properties of multifunctional cementitious composites, J. Nanomater. 2020 (2020) 6749150, https://doi.org/10.1155/2020/6749150.
[88] P.C. Ma, J.-K. Kim, B.Z. Tang, Functionalization of carbon nanotubes using a silane coupling agent, Carbon N. Y. 44 (2006) 3232–3238, https://doi.org/10.1016/j.carbon.2006.06.032.
[89] P.-C. Ma, N.A. Siddiqui, G. Marom, J.-K. Kim, Dispersion and functionalization of carbon nanotubes for polymer-based nanocomposites: a review, Compos. Part A Appl. Sci. Manuf. 41 (10) (2010) 1345–1367.
[90] L.-C. Tang, Y.-J. Wan, D. Yan, Y.-B. Pei, L. Zhao, Y.-B. Li, L.-B. Wu, J.-X. Jiang, G.-Q. Lai, The effect of graphene dispersion on the mechanical properties of graphene/epoxy composites, Carbon N. Y. 60 (2013) 16–27, https://doi.org/10.1016/j.carbon.2013.03.050.
[91] J. Han, J. Pan, J. Cai, X. Li, A review on carbon-based self-sensing cementitious composites, Constr. Build. Mater. 265 (2020) 120764, https://doi.org/10.1016/j.conbuildmat.2020.120764.
[92] B. Han, K. Zhang, X. Yu, E. Kwon, J. Ou, Fabrication of piezoresistive CNT/CNF cementitious composites with superplasticizer as dispersant, J. Mater. Civ. Eng. 24 (2012) 658–665, https://doi.org/10.1061/(ASCE)MT.1943-5533.0000435.
[93] B.H. Ter Meulen, Industrial Tpu applications in Europe, J. Coat. Fabr. 12 (3) (1983) 148–159.
[94] F.B. Walter, Thermoplastic polyurethanes—a versatile material for industrial fabric application, J. Coat. Fabr. 7 (4) (1978) 293–307.
[95] E. Paz, M. Jiménez, L. Romero, M. del M. Espinosa, M. Domínguez, Characterization of the resistance to abrasive chemical agents of test specimens of thermoplastic elastomeric polyurethane composite materials produced by additive manufacturing, J. Appl. Polym. Sci. 138 (2021) 50791.
[96] D. Janczak, M. Zych, T. Raczyński, Ł. Dybowska-Sarapuk, A. Pepłowski, J. Krzemiński, A. Sosna-Głębska, K. Znajdek, M. Sibiński, M. Jakubowska, Stretchable and washable electroluminescent display screen-printed on textile, Nanomaterials 9 (9) (2019) 1276.
[97] G. Mármol, U.K. Sanivada, R. Fangueiro, Effect of GNPs on the piezoresistive, electrical and mechanical properties of PHA and PLA films, Fibers 9 (2021) 86.
[98] U.K. Sanivada, D. Esteves, L.M. Arruda, C.A. Silva, I.P. Moreira, R. Fangueiro, Joule-heating effect of thin films with carbon-based nanomaterials, Materials (Basel) 15 (2022) 4323.
[99] R. Polo-Mendoza, T. Navarro-Donado, D. Ortega-Martinez, E. Turbay, G. Martinez-Arguelles, R. Peñabaena-Niebles, Properties and characterization techniques of graphene modified asphalt binders, Nanomaterials 13 (2023) 955.
[100] E. Turbay, G. Martinez-Arguelles, T. Navarro-Donado, E. Sánchez-Cotte, R. Polo-Mendoza, E. Covilla-Valera, Rheological behaviour of WMA-modified asphalt binders with crumb rubber, Polymers (Basel) 14 (2022) 4148.
[101] R. Polo-Mendoza, G. Martinez-Arguelles, L.F. Walubita, F. Moreno-Navarro, F. Giustozzi, L. Fuentes, T. Navarro-Donado, Ultraviolet ageing of bituminous materials: a comprehensive literature review from 2011 to 2022, Constr. Build. Mater. 350 (2022) 128889.
[102] A. Katz, V.C. Li, Bond properties of micro-fibers in cementitious matrix, MRS Online Proc. Libr. 370 (1994).
[103] A. Peled, E. Zaguri, G. Marom, Bonding characteristics of multifilament polymer yarns and cement matrices, Compos. Part A Appl. Sci. Manuf. 39 (2008) 930–939, https://doi.org/10.1016/j.compositesa.2008.03.012.
[104] S. Ghosh, S. Remanan, S. Mondal, S. Ganguly, P. Das, N. Singha, N.C. Das, An approach to prepare mechanically robust full IPN strengthened conductive cotton fabric for high strain tolerant electromagnetic interference shielding, Chem. Eng. J. 344 (2018) 138–154, https://doi.org/10.1016/j.cej.2018.03.039.
[105] P. Cataldi, L. Ceseracciu, A. Athanassiou, I.S. Bayer, Healable cotton-graphene nanocomposite conductor for wearable electronics, ACS Appl. Mater. Interfaces. 9 (2017) 13825–13830, https://doi.org/10.1021/acsami.7b02326.
[106] U.K. Sanivada, G. Mármol, R. Fangueiro, in: Hierarchical Vegetal Fiber Reinforced Composites BT - Vegetable Fiber Composites and their Technological Applications, Springer Singapore, Singapore, 2021, pp. 379–412, https://doi.org/10.1007/978-981-16-1854-3_17.
[107] P. Jusner, E. Schwaiger, A. Potthast, T. Rosenau, Thermal stability of cellulose insulation in electrical power transformers – a review, Carbohydr. Polym. 252 (2021), 117196, https://doi.org/10.1016/j.carbpol.2020.117196.
[108] R. Marzouki, A. Brahmia, S. Bondock, S.M.A.S. Keshk, M.F. Zid, A.G. Al-Sehemi, A. Koschella, T. Heinze, Mercerization effect on structure and electrical properties of cellulose: development of a novel fast Na-ionic conductor, Carbohydr. Polym. 221 (2019) 29–36.
[109] M. Yang, J. Pan, A. Xu, L. Luo, D. Cheng, G. Cai, J. Wang, B. Tang, X. Wang, Conductive cotton fabrics for motion sensing and heating applications, Polymers (Basel) 10 (6) (2018) 568.
[110] M.J. Rahman, M.F. Hossain, M.J. Islam, T. Mieno, M.N. Chowdhury, Carbon nanotube reinforced natural rubber nanocomposite as a stretchable electronic material, J. Mater. Eng. Perform. 1–8 (2022).
[111] A. Ahmed, M.A. Jalil, M.M. Hossain, M. Moniruzzaman, B. Adak, M.T. Islam, M. S. Parvez, S. Mukhopadhyay, A PEDOT:PSS and graphene-clad smart textile-based wearable electronic Joule heater with high thermal stability, J. Mater. Chem. C 8 (2020) 16204–16215, https://doi.org/10.1039/D0TC03368E.
[112] H. Souri, D. Bhattacharyya, Highly stretchable multifunctional wearable devices based on conductive cotton and wool fabrics, ACS Appl. Mater. Interfaces. 10 (2018) 20845–20853, https://doi.org/10.1021/acsami.8b04775.
[113] X. Hu, M. Tian, L. Qu, S. Zhu, G. Han, Multifunctional cotton fabrics with graphene/polyurethane coatings with far-infrared emission, electrical conductivity, and ultraviolet-blocking properties, Carbon N. Y. 95 (2015) 625–633, https://doi.org/10.1016/j.carbon.2015.08.099.
[114] P. Pereira, D.P. Ferreira, J.C. Araújo, A. Ferreira, R. Fangueiro, The potential of graphene nanoplatelets in the development of smart and multifunctional ecocomposites, Polymers (Basel). 12 (10) (2020) 2189.
[115] F. Tomczak, K.G. Satyanarayana, T.H.D. Sydenstricker, Studies on lignocellulosic fibers of Brazil: Part III – morphology and properties of Brazilian curauá fibers, Compos. Part A Appl. Sci. Manuf. 38 (2007) 2227–2236, https://doi.org/10.1016/j.compositesa.2007.06.005.
[116] K.G. Satyanarayana, J.L. Guimarães, F. Wypych, Studies on lignocellulosic fibers of Brazil. Part I: Source, production, morphology, properties and applications, Compos. Part A Appl. Sci. Manuf. 38 (2007) 1694–1709, https://doi.org/10.1016/j.compositesa.2007.02.006.
[117] M. Parvinzadeh, I. Ebrahimi, Influence of atmospheric-air plasma on the coating of a nonionic lubricating agent on polyester fiber, Radiat. Eff. Defects Solids 166 (2011) 408–416, https://doi.org/10.1080/10420150.2011.553230.
[118] I.M. De Rosa, J.M. Kenny, D. Puglia, C. Santulli, F. Sarasini, Morphological, thermal and mechanical characterization of okra (Abelmoschus esculentus) fibres as potential reinforcement in polymer composites, Compos. Sci. Technol. 70 (2010) 116–122, https://doi.org/10.1016/j.compscitech.2009.09.013.
[119] E.H. Portella, D. Romanzini, C.C. Angrizani, S.C. Amico, A.J. Zattera, Influence of stacking sequence on the mechanical and dynamic mechanical properties of cotton/glass fiber reinforced polyester composites, Mater. Res. 19 (2016) 542–547.
[120] Z. Zhao, J. Zhou, T. Fan, L. Li, Z. Liu, Y. Liu, M. Lu, An effective surface modification of polyester fabrics for improving the interfacial deposition of polypyrrole layer, Mater. Chem. Phys. 203 (2018) 89–96, https://doi.org/10.1016/j.matchemphys.2017.09.062.
[121] D. Romanzini, H.L. Ornaghi Junior, S.C. Amico, A.J. Zattera, Preparation and characterization of ramie-glass fiber reinforced polymer matrix hybrid composites, Mater. Res. 15 (2012) 415–420.
[122] N. Sgriccia, M.C. Hawley, M. Misra, Characterization of natural fiber surfaces and natural fiber composites, Compos. Part A Appl. Sci. Manuf. 39 (2008) 1632–1637, https://doi.org/10.1016/j.compositesa.2008.07.007.
[123] T.-C. Lin, D.-J. Lee, Cotton fabrics modified for use in oil/water separation: a perspective review, Cellulose 28 (2021) 4575–4594.
[124] Y. Jia, Y.i. Lu, G. Zhang, Y. Liang, F. Zhang, Facile synthesis of an eco-friendly nitrogen–phosphorus ammonium salt to enhance the durability and flame retardancy of cotton, J. Mater. Chem. A 5 (20) (2017) 9970–9981.
[125] T. Gou, X. Wu, Q. Zhao, S. Chang, P. Wang, Novel phosphorus/nitrogen-rich oligomer with numerous reactive groups for durable flame-retardant cotton fabric, Cellulose 28 (2021) 7405–7419, https://doi.org/10.1007/s10570-021-03980-x.
[126] M.M. Kamel, M.M. El Zawahry, H. Helmy, M.A. Eid, Improvements in the dyeability of polyester fabrics by atmospheric pressure oxygen plasma treatment, J. Text. Inst. 102 (2011) 220–231, https://doi.org/10.1080/00405001003672366.
[127] D. Shao, Q. Wei, Microwave-assisted rapid preparation of nano-ZnO/Ag composite functionalized polyester nonwoven membrane for improving its UV shielding and antibacterial properties, Mater 11 (8) (2018) 1412.
[128] G. Trovati, E.A. Sanches, S.C. Neto, Y.P. Mascarenhas, G.O. Chierice, Characterization of polyurethane resins by FTIR, TGA, and XRD, J. Appl. Polym. Sci. 115 (2010) 263–268, https://doi.org/10.1002/app.31096.
[129] M.T. Parizi, G.R. Ebrahimi, H.R. Ezatpour, M. Gupta, J. Li, W.H. Guo, Trimodal hierarchical structure in the carbonaceous hybrid (GNPs+ CNTs) reinforced CoCrFeMnNi high entropy alloy to promote strength-ductility synergy, Mater. Sci. Eng. A 850 (2022) 143446.
[130] T.A. V Abdullah, Ö.Z. Yahya, H.İ. AKYILDIZ, Thermal and Mechanical Properties of Sol-Gel Silica Coated Fabrics, Avrupa Bilim ve Teknol. Derg. (2021) 309–319.
[131] A. Bentur, S. Mindess, Fibre reinforced cementitious composites, CRC Press, 2006.
[132] Z. Lin, T. Kanda, V.C. Li, On interface property characterization and performance of fiber reinforced cementitious composites, (1999).
[133] A. Peled, A. Bentur, Quantitative description of the pull-out behavior of crimped yarns from cement matrix, J. Mater. Civ. Eng. 15 (6) (2003) 537–544.
[134] M. Abedi, O. Hassanshahi, A. Rashiddel, H. Ashtari, M.S. Meddah, D. Dias, M.A. Arjomand, K.K. Choong, Investigation of Mechanical Behavior of a Sustainable Cementitious Composite Reinforced with Natural Fibre: An Experimental and Numerical Study, Available SSRN 4247583. (n.d.).
[135] Y. Jin, X. Zhou, M. Chen, Z. Zhao, Y. Huang, P. Zhao, L. Lu, High toughness 3D printed white Portland cement-based materials with glass fiber textile, Mater. Lett. 309 (2022) 131381, https://doi.org/10.1016/j.matlet.2021.131381.
[136] B. Han, S. Ding, X. Yu, Intrinsic self-sensing concrete and structures: a review, Measurement 59 (2015) 110–128, https://doi.org/10.1016/j.measurement.2014.09.048.

[137] D.D.L. Chung, Carbon composites: composites with carbon fibers, nanofibers, and nanotubes, in: Carbon Composites, Elsevier, 2017, pp. 1–87.
[138] M. Abedi, R. Fangueiro, A.G. Correia, Effects of electrodes layout and filler scale on percolation threshold and piezoresistivity performances of a cementitious-based geocomposite, Nanomaterials 12 (2022) 1734. https://www.mdpi.com/2079-4991/12/10/1734.
[139] A. Bazargan, G. McKay, A review – synthesis of carbon nanotubes from plastic wastes, Chem. Eng. J. 195–196 (2012) 377–391, https://doi.org/10.1016/j.cej.2012.03.077.
[140] N. Borsodi, A. Szentes, N. Miskolczi, C. Wu, X. Liu, Carbon nanotubes synthetized from gaseous products of waste polymer pyrolysis and their application, J. Anal. Appl. Pyrolysis 120 (2016) 304–313, https://doi.org/10.1016/j.jaap.2016.05.018.
[141] S. Ren, X. Xu, K. Hu, W. Tian, X. Duan, J. Yi, S. Wang, Structure-oriented conversions of plastics to carbon nanomaterials, Carbon Res. 1 (2022) 15.
[142] R. Polo-Mendoza, G. Martinez-Arguelles, R. Peñabaena-Niebles, Environmental optimization of warm mix asphalt (WMA) design with recycled concrete aggregates (RCA) inclusion through artificial intelligence (AI) techniques, Results Eng. 17 (2023) 100984.
[143] L.F. Walubita, G. Martinez-Arguelles, R. Polo-Mendoza, S. Ick-Lee, L. Fuentes, Comparative environmental assessment of rigid, flexible, and perpetual pavements: a case study of Texas, Sustainability 14 (2022) 9983.
[144] R. Polo-Mendoza, G. Martinez-Arguelles, R. Peñabaena-Niebles, A multi-objective optimization based on genetic algorithms for the sustainable design of Warm Mix Asphalt (WMA), Int. J. Pavement Eng. 1–21 (2022).